Characterisation of proton exchange membranes using a high-pressure gas membrane rupture test

W Kirsten

22129235

Dissertation submitted in fulfilment of the requirements for the degree *Magister* in Chemical Engineering at the Potchefstroom Campus of the North-West University

Supervisor: Prof HWJP Neomagus

Co-supervisor: Dr DG Bessarabov

May 2016

Page left black intentionally

Acknowledgements

I wish to thank my supervisors Prof. Hein Neomagus and Dr. Dmitri Bessarabov for everything they have offered me in the past two years. They served as mentors by the definition of the word and their wisdom, encouragement and patients will always be appreciated. Both are sources to ideas in this dissertation, for which I am grateful to.

I appreciate Dr. Andries Kruger's continuous support and guidance. I especially want to thank him for numerous discussions on problems I encountered and never shying away from lending a helping hand and being a true friend when times got hard.

A special word of appreciation to Jan-Hendrik van der Merwe who mentored me through my graduate degree, inspired me to pursue a post graduate degree and never stopped believing in me.

I am grateful to the rest of the HySA infrastructure Centre of Competence research team (Dr. Steven Chuita, Gerhard Human, Faan Oelofse and Neels le Roux) who provided inspiration, insight and friendship through the past two years and Ted Paarlberg for the construction of the experimental rig.

Thanks must go to HySA Infrastructure Centre of Competence for valuing my work and providing financial support.

I would also like to thank IMP calibration services™ for allowing me to use their facilities in order to complete this dissertation.

My friends and family have provided me with the strongest support since I started this long journey. I will forever be in your debt. You inspire me everyday and I hope that I have made you proud through this work. Everyone has a share in every accomplishment I make.

Abstract

Keywords: Nafion®, Proton Exchange Membrane, Membrane Rupture Test, Biaxial Strength, Young's modulus, Cation Contamination, Relative Humidity and Temperature.

The purpose of this research was to investigate the effect of operational environmental parameters of electrochemical hydrogen energy systems on the mechanical and viscoelastic properties of Proton Exchange Membranes through the use of a high-pressure gas membrane rupture test rig.

A biaxial tensile testing method was proposed to characterise the viscoelastic properties that affect the mechanical durability of proton exchange membranes. It served as a good representation of the operational environment found within electrochemical hydrogen energy systems, replicating stresses induced on the constrained membranes. Through the use of a high-pressure gas membrane rupture test the rupture pressure and membrane defection were recorded, enabling the determination of the Young's modulus. The values obtained from the biaxial testing were compared to results obtained through uniaxial tensile testing at the same environmental conditions and agreement between the two methods was obtained.

It was observed that the Young's modulus remains constant for all Nafion® materials at a fixed environmental condition, regardless of the thickness of the membrane specimen. The high-pressure membrane rupture test was used to determine the Young's modulus of Nafion® membranes at three temperatures (20 ℃, 50 ℃ and 80 ℃) and four relative humidity levels (35 %, 50 %, 70 % and 90 %). The results showed that the Young's modulus decreases with increased temperature and RH with the change in temperature having a significantly larger effect.

The biaxial tensile testing was also used for the determination of the ultimate membrane stress at the point of rupture. By using a mathematical model proposed by Schomburg (2011) it was possible to show that during the membrane rupture test there are no influence of bending moments on the total stress of the membrane. It was also shown that all initial residual stresses are negligibly small.

Nafion® 1110 membrane samples were found to have a higher rupture pressure at sub-zero temperatures than at the studied temperature larger than 0 ℃. It was also shown that the properties of the membrane remain constant for the two temperatures.

Nafion® 1110 membranes were subjected to ion exchange with cations (Na^{+}, Mg^{2+} and Fe^{3+}). An increase in the Young's modulus was observed with the presence of foreign cations as a result of reduced moisture uptake.

Reinforced membranes were ruptured at 90 % RH and 50 ℃ with the rupture pressures compared to Nafion® membranes with similar thicknesses at the same environmental conditions. The rupture pressure of the reinforced membranes showed a nearly 100 % increase in strength compared to that of the Nafion® membranes. It is therefore clear that the e-PTFE layer of the reinforced membranes strongly improves the mechanical strength of the specimen.

Unhydrolyzed perfluorinated membranes were partially hydrolysed for up to 46 hours to investigate the effect of the equivalent weight of the membrane specimen on the mechanical strength. These tests showed that the equivalent weight of the specimens decreased as the hydrolysis time increased, which in turn resulted in an increase of the rupture pressure of the specimen at 50 % RH and 50 ℃.

List of Presentations and Publications

Kirsten, W., Kruger, A.J.K, Bessarabov, D.G & Neomagus, H.W.J.P. 2014. Gen 1 high-pressure membrane rupture test for electrochemical hydrogen compression system. Poster presented at Catalysis Society of South-Africa Annual conference. (Conference presentation).

Kirsten, W., Bessarabov, D.G & Neomagus, H.W.J.P. 2015. Biaxial strength characterisation of proton exchange membranes using a high-pressure gas membrane rupture test. Poster presented at Catalysis Society of South-Africa Annual conference. (Conference presentation).

Table of Content

List of Figures

List of Tables

List of Symbols

Nomenclature

A_0	Original Cross Sectional Area Through Which Force Is Applied (mm^2)
d_M	Membrane thickness (mm)
E	Young's modulus / Young's Modulus (MPa)
F	Force Exerted Under Tension (kN)
F_F	Force of the frame (kN)
F_P	Total force (kN)
L	Deflection Length (mm)
L_0	Original Length of The Object (mm)
ΔL_T	Change of Length During Uniaxial Testing (mm)
$M_{membrane}$	Mass of dry membrane in H^+- ionic form (g)
N_{st}	Standard concentrations of HCl and NaOH used (M)
ΔP	Pressure differential (MPa)
$P_{Rupture}$	Rupture pressure (MPa)
R_M	Radius (mm)
T_d	Drying Temperature (°C)
T_h	Humidification Temperature (°C)
V_{HCl}	Volume of HCl solution used for titration (ml)
V_{IE}	Volume of HCl used for ion exchange (ml)
V_{NaOH}	Volume of titrated NaOH solution (ml)
w_0	Deflection (mm)

Greek symbols

ε	Extensional Strain (MPa)
ε_R	Radial Strain (MPa)
ε_T	Tangential Strain (MPa)
σ	Tensile Stress (MPa)
σ_0	Initial Stress (MPa)
σ_M	Membrane Stress (MPa)
σ_R	Radial Stress (MPa)
$\sigma_{R(max)}$	Maximum radial stress / ultimate stress (MPa)

σ_T	Tangential Stress (MPa)
ν_m	Poisson's Ratio

List of Abbreviations

DIW	Deionised Water
DSC	Differential Scanning Calometry
EHC	Electrochemical Hydrogen Compression
EW	Equivalent Weight (g [dry membrane in H^+- ionic form] / mol.SO_3^-)
ePTFE	Expanded Polytetrafluoroethylene
FLOW	Flow Meter
P-REG	Front Pressure Regulator
IC	Internal Combustion
IEC	Ion Exchange Capacity (mol.SO_3^-/ g [dry membrane in H^+ ionic form])
LSC	Long Side Chain
MD	Machine Direction
NV	Needle Valve
OEM	Original Equipment Manufacturer
PFSA	Perfluorosulfonic Acid
PFSI	Perfluorosulfonic Ionomers
PTFE	Polytetrafluoroethylene
PRV	Pressure Relief Valve
PEM	Proton Exchange Membrane
PEMFC	Proton Exchange Membrane Fuel Cell
RH	Relative Humidity
SSC	Short Side Chain
SV	Solenoid Valve
SS	Stainless Steel
TD	Transverse Direction

Chapter 1 - Introduction

A brief introduction to the background of this study is provided in this chapter. This includes information on the field of electrochemical hydrogen energy system and the motivation for this project. Thereafter, the aims and objectives of this work are given followed by the layout of the dissertation.

1.1. Background

As fossil fuel deposits continue to deplete, research and utilisation of alternative energy carriers such as wind, nuclear and hydrogen become increasingly necessary (Rohland *et al.*, 1998). Interest in hydrogen as a fuel source has grown strongly, since 1990, due to the advantages as an energy carrier. Hydrogen has the highest energy density by weight of any common fuel, and can be produced renewably from a variety of (non-fossil) feedstock (Yang *et al*., 2010).

In order to create a fully functional hydrogen infrastructure that is economically viable, hydrogen-production, storage and technologies have to be researched and improved (Rohland *et al*., 1998). Creating this network is key in providing the fuel needed for starting the transition to transport using alternative fuel sources such as fuel cell operated vehicles.

Electrochemical hydrogen energy systems which form part of the above mentioned hydrogen infrastructure include electrochemical compressors, hydrogen fuel cells and water electrolysers (Oda *et al.,* 1987 and Yang *et al.,* 2010). Proton Exchange Membranes (PEM) are at the heart of each technology, with perfluorosulfonic acid (PFSA) membranes the most commonly used in these specialised applications (Luo, 2007). Nafion® membranes are the most favoured of PFSA membranes due to their high proton conductivity, low electronic resistance, good mechanical properties, low gas permeability and excellent chemical stability (Solasi *et al.,* 2007, Tang *et al*., 2007 and Solasi *et al.,* 2010).

Within these systems the PEM is subject to degradation and it is necessary to have a fundamental understanding of the mechanical and viscoelastic properties of the materials under operational conditions to ensure safe operation (Collier *et al.,* 2006). The degradation of the membrane is caused by electrochemical and mechanical stresses within the membrane, which are introduced within the operational environment and result in membrane thinning, tensile strength loss and pinhole formation (Bessarabov and Kozak, 2007). These stresses mainly result from large pressure differences, variation of temperature and relative humidity (RH), charge modulus, cation contamination, hydroxy- and peroxy- radical formation and oxygen activation (Bessarabov and Kozak, 2007., Collier *et al.,* 2006, Inaba *et al.,* 2006 and Vengatesan *et al.,* 2011).

By understanding the behaviour of the membrane material under these stresses, it is possible to better understand the degradation of the material (Cheng *et al.,* 2007). This in turn leads to progress on improving the durability of the membranes within a working electrochemical hydrogen energy system, which is considered one of the main characteristics preventing large scale deployment of these technologies (Wu *et al.* 2008).

Although the use of various membranes are widespread and the chemical and electrochemical degradation of perfluorinated membranes have been investigated and reported extensively, little work has been published on mechanical degradation of membranes (Bessarabov *et al.,* 2007 and Solasi *et al*., 2007). As a result, significant gaps remain in understanding the mechanical behaviour of these materials (Solasi *et al.,* 2007, Tang *et al.,* 2007, Wu *et al,*. 2008, Li *et al*., 2009, Solasi *et al.,* 2010, Shi *et al.,* 2013 and Moukheiber *et al*., 2014).

In addition, several researchers have pointed out that there is a dearth of comprehensive information about the viscoelastic properties of membranes, particularly at elevated temperatures and humidity (Satterfield, 2008). The available information is fragmented as a result, leaving the researcher with incomparable data. It is therefore imperative to create a data set that represents the viscoelastic properties of proton exchange membranes over an extensive range of environmental conditions.

Electrochemical hydrogen energy systems are not operated at sub-zero temperatures, however it is requirement of the technologies to be able to initiate start up at such conditions. Information on the mechanical integrity and viscoelastic properties of the proton exchange membranes at these temperatures are not available in literature. In addition the effect of cation contaminants on the viscoelastic properties of proton exchange membranes along with the strength of and partially hydrolysed membranes have not been studied extensively. As a result, it is necessary to investigate these variables to further improve the understanding of proton exchange materials

1.2. Aim and objectives

The aim of the project is to construct a complete data set of the Young's modulus of proton exchange membranes over an extensive range of temperatures and relative humidity levels. Further, it is the aim to determine how the Young's modulus and mechanical integrity of proton exchange membranes are influenced by the presence of foreign cations and the presence of mechanical reinforcement.

The objectives are:

- Develop, construct and validate a high pressure gas membrane rupture test under environmentally controlled conditions.
- Determine the Young's modulus of Nafion® membrane using the developed method.
- Investigate the influence of temperature, relative humidity and cation contamination on the viscoelastic properties of reinforced and non-reinforced proton exchange membranes.
- Investigate the influence of the degree of hydrolysis on the viscoelastic properties of non - hydrolysed membranes by partially hydrolysing the membranes.

1.3. Layout of dissertation.

In Chapter 2 an overview of proton exchange membranes used within electrochemical hydrogen energy systems is given along with methods currently used for determining mechanical and viscoelastic properties of these materials. Further, a review on the most relevant work in the field of viscoelastic properties of PFSA membranes is included. In Chapter 3 information regarding the experimental step and procedures is discussed. This includes a summary of the materials, equipment and all experimental procedures. The results obtained through experimental work are discussed and compared to literature in Chapter 4. Finally, the conclusions drawn from the results and recommendations for future work on the characterisation of PEMs are provided in Chapter 5.

Chapter 2 - Literature review

An overview of proton exchange membranes utilised within electrochemical hydrogen energy systems such as hydrogen fuel cells, electrolysis and electrochemical hydrogen compressors is given in this Section 2.1. Thereafter, methods used in the determination of mechanical and viscoelastic properties of membrane materials will be explored in Section 2.2. This includes advantages and methodology on the use of biaxial tensile testing. The chapter is concluded with a review of work published on viscoelastic properties of thin polymer membranes over an extensive range of environmental conditions in Section 2.3, with emphasis placed on the Young's modulus of Nafion®.

2.1. Proton exchange membrane materials

2.1.1. Non-reinforced membranes

Catalyst coated proton exchange membranes are essentially the heart of electrochemical hydrogen systems (Luo, 2007). Due to the diversity of these systems, PEMs have evolved over time to better suit specific operational parameters. The variety of PEMs include perfluorosulfonic acid (PFSA) membranes, phosphoric acid membranes, hydrocarbon-based sulfonated membranes and polybenzimidazole (PBI) membranes (Bessarabov *et al.,* 2000, Bessarabov & Kozak, 2007, Onda *et al.,* 2007 Rikukawa & Sanui, 2000 and Thomassem *et al.,* 2010). Each specimen has a slightly different chemical structure which affects the behaviour of the material's proton conductivity, water distribution and functionality at different temperatures and RH levels.

Within membrane-based electrochemical hydrogen energy systems such as electrolysers, electrochemical hydrogen compressors and hydrogen fuel cells operated at temperatures below 80 ℃, PFSA membranes are most commonly used due to its high proton conductivity, good mechanical properties, low electronic resistance, low gas permeability and excellent chemical stability (Solasi *et al.,* 2007, Tang *et al*., 2007 and Solasi *et al.,* 2010). Due to its versatility, PFSA materials can consist of both short and long side chain segments to enhance the performance of the composite membranes (Moukheiber *et al.,* 2014). These compositional and structural changes impact specific properties. Short side chain (SSC) PFSA membranes have high ion exchange capacity (IEC), high crystallinity, and moreover excellent thermal and chemical stability. Conversely, the long-side chains (LSC) affect the membrane microstructures, such as ion cluster size, density, and distribution, thus giving the new membranes unique and excellent performance (Moukheiber *et al.,* 2014).

The membrane most favoured among the PFSA polymers, used within PEM technologies, is the sulfonated tetrafluoroethylene copolymer with the trade name Nafion®, originally developed and manufactured by DuPont in the 1960's (Grot, 2008). Nafion® membranes are considered to be the benchmark of PEMs and are the most widely used membranes in low temperature electrochemical applications (Rohland *et al.,* 1998). Nafion® possesses a strong phase-segregated backbone with pendent side chains, of which the structure evolves during hydration. The chemical stability and structural integrity of Nafion® can be contributed to the strongly bound hydrophobic perfluorinated backbone, while its high proton conductivity when hydrated can be contributed to the hydrophilic perfluorosulfonic acid side chains (Andrews *et al.,* 2013). The chemical structure of short side chain (SSC) and long side chain (LSC) PFSA membranes are presented in Figure 2.1.

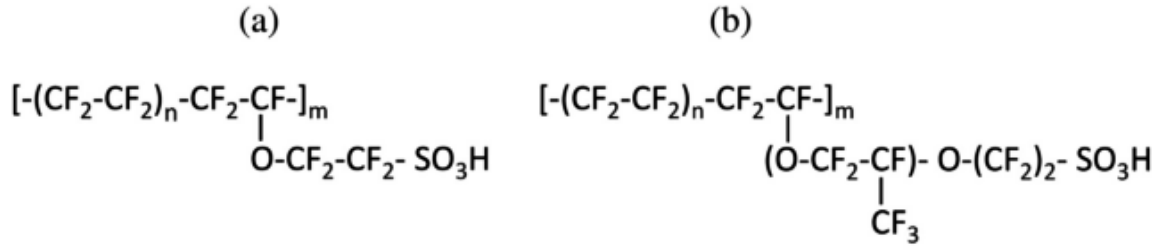

Figure 2.1 - Chemical structure of PFSA membrane - (a) Short side Chain (SSC) type membrane, (b) Long Side Chain (LSC) type membrane.

Nafion® membranes are available in different sizes and thicknesses to accommodate the technology it is used in. The material is fabricated by extrusion or solution casting, with solution casting being the preferred method for the fabrication of thinner films (<50 μm) (Grot, 2008). Electrochemical hydrogen energy systems have different operational parameters (pressure, temperature and hydration levels) best suited to the technology and specific membrane type (Ito *et al.,* 2011). Each Nafion® membrane is categorised by the letter N followed by a three or four digit number. The first two and last two digits represent the equivalent weight divided by 100 and the membrane thickness respectively. Nafion® is available in 2, 3.5, 5, 7 & 10 mill respectively (1 mill = 0.0254 mm) (DuPont, 2015). True Nafion® solutions are very difficult to obtain, therefore the molecular weight cannot be determined by common methods like light scattering and gel permeation chromatography (Barbir, 2013). The equivalent weight (EW), defined as the gram of dry polymer per number of moles of sulfonic acid groups (g.polymer/mol SO_3H) is generally used as the basis of comparison between ionomer membranes (Barbir, 2013).

The ion conductivity, morphology, viscoelastic properties and mechanical properties of the material are strong functions of the polymer's water content. The water content in return is a function of the equivalent weight, source of humidification and the pre-treatment history (Zhang & Shen, 2012). As the EW decreases, the concentration of ionic groups present in the polymer increases resulting in larger interaction with the solvent (Grot, 2008). Furthermore, studies show that liquid water is superior to vapour water as a humidification source, as a greater water uptake is observed within the same time-frame (Maldonado *et al.*, 2012). The water uptake is also affected by the humidification temperature (T_h) (Maldonado *et al.,* 2012). An increase in water uptake is observed at increased humidification temperatures, as a result of increased softening at elevated temperatures (Solasi *et al.,* 2010).

One of the most important properties of Nafion® is its ability to provide an ionic path for proton transport through the membrane (Moukheiber *et al.*, 2012). As the hydration level of the membrane is increased, the ionic domains swell to form a percolated network (Zhang & Shen, 2012). The channels that develop are well-connected and act as conductive pathways that promotes the mobility of ions throughout the film. The excellent performance of Nafion® as an ion conducting material can be contributed to the strong phase-segregated morphology (Shi *et al.,*

2013). Therefore, an increase in hydration promotes proton conduction (Petrina, 2013). However, when Nafion® films are insufficiently hydrated or dry, the ionic domains are isolated from one another, resulting in poor conduction through the film (Zhang & Shen, 2012). The water within the hydrophilic domains reduce the strength of electrostatic bonds between sulfonate groups causing the polymer chains to plasticise (Liu *et al.,* 2006). The ionic domains swell, which causes internal pressure on the matrix. If the water content in the membrane is too high, the water will start to accumulate and condense within the membrane, leading to excessive swelling of the membrane and resulting in decreased ion mobility (Choi *et al.,* 2006).

During normal operation of electrochemical hydrogen devices, the humidity and temperature are frequently altered, causing the membrane to dehydrate and rehydrate repeatedly. This leads to deterioration of the membrane, affecting the performance of the electrochemical device. For this reason, a great deal of focus has been placed on the reinforcement of these membranes, to marginalise the deterioration (Shi *et al., 2013).*

2.1.2. Reinforced membranes

Reinforced ionomer membranes for hydrogen technologies are new-age membranes introduced recently (Barbir, 2013, Gore, 1976 and Gore, 1980). Instead of being composed of a homogeneous PFSA material, reinforced membranes are composed of a matrix consisting of an expanded polytetrafluoroethylene (ePTFE) backing in conjunction with a thinner PFSA material. The ePTFE backing provides the membranes with improved mechanical properties (Gore, 1976, Gore, 1978 and Hockday, 1995).

Mechanical reinforcement with expanded PTFE sheets are usually combined with thinner membranes and provide much greater mechanical strength, increased membrane conductance, reduced permeability, improved water distribution, less dimensional variation and improved performance without sacrificing durability compared to non-reinforced membranes (Grot, 2008, Hockday, 1995). Although mechanical reinforcement can extend the lifetime, there is no clear understanding of the mechanisms that govern the mechanical behaviour of the reinforced material compared to the non-reinforced one (Gore 1976, Moukheiber *et al.* 2014 and Wu *et al.* 2014).

Expanded polytetrafluoroethylene (ePTFE), introduced by W.L. Gore & Associates Inc. in 1976 as GORE-TEX (Gore, 1976 and Gore, 1978), is most commonly used as porous support for reinforced membranes. The increase in strength of the polymer matrix is highly dependent on the properties of material prior to expansion, the polymers degree of crystallinity, the temperature and rate at which the expansion is performed and the amorphous locking methods used (Gore, 1976). Expansion at high temperatures and high expansion rates causes the structure of the polymer to become more homogeneous with more closely spaced nodes, interconnected with a greater number of fibrils resulting in increased mechanical strength (Gore, 1976). Therefore, the

expansion causes the polymer to share physical stress and prevent the formation of crossover pathways (Patil *et al.* 2010).
Another method for making a reinforced polymer electrolyte membranes is presented by Guerra *et al.* (2008). The authors proposed chemical reinforcement, by mixing a sulfonate- or sulfonyl halide-functional polymer with a bisamidine compound and subsequently trimerizing the maiden groups of the bisamidine compound to form triazine linkages. A polymer electrolyte reinforced with a polytriazine is yielded.

The use of ePTFE and chemical reinforcement are only two examples of a membrane reinforcement techniques (Guerra *et al.*, *2008* Hockday, 1995). Due to the commercialisation of membranes most methods and compositions of membranes are kept discrete and unpublished as they are trade secrets.

2.2. Bulge/blister testing

Numerous methods are available for the measurement of the mechanical and viscoelastic properties of materials such as the uniaxial tensile test, cantilever beam bending test, nano indentation and frequency resonant test (Wu *et al.,* 2000). Of these methods tensile testing is the most commonly used method for the determination of mechanical properties, as it can be implemented in the testing of materials ranging from steel to hair fibres (Campos *et al.,* 2014). However, when the materials are extremely thin or small it is difficult to conduct the tests without specialised equipment as there are issues with sample alignment and gripping (Wu *et al.,* 2000). Therefore, mechanical testing of thin films required novel thinking that can incorporate the geometry and microstructure of the samples.

Based on the reasons above, a testing frame approach was established to measure the mechanical properties of thin film materials such as Young's modulus, residual stresses and adhesive strength. This method is known as bulge/blister testing. The experimental technique of the bulge/blister test was first introduced by Beams (1959) where the mechanical properties of polycrystalline and single-crystal gold and silver films deposited on a substrate were determined using the assumption of the spherical cap model. Interest in the use of bulge/blister testing grew through the 1980's due to the development of the semiconductor industry, allowing micro-machining methods to be made easily available (Merle, 2013). These methods were used to assist in the reduction of the complexity of fabrication of free standing samples, although it was essentially only used for producing square and rectangular samples. As a result, researchers promoted the use of rectangular shaped samples, leading to a better understanding of plane-strain, plane-stress and uniaxial stress which are all used in studies involving plastic deformation of materials (Merle, 2013).

Bulge/blister testing has been used to some extent to determine the biaxial mechanical properties of materials. When compared to standard uniaxial tensile testing a higher range of deformation is

permitted, resulting in better characterisation of materials whilst allowing fewer discrepancies with regards to data exploration (Campos *et al.,* 2014). Edwards *et al.* (2004) incorporated the bulge/ blister testing method to characterise thin films of silicon nitrate with the use of air as pressure medium and Campos *et al.* (2014) used the method for the characterisation of thin metal sheet films with the use of oil as pressurisation medium. Li *et al.* (2009) proposed the use of a pressure-loaded blister/bulge test configuration for the characterisation of biaxial mechanical properties of proton exchange membranes over a range of environmental conditions and loading profiles. This configuration has been used in several studies in the characterisation of other membranes and thin films (Campos *et al.,* 2014, Edwards *et al.,* 2004, Jia *et al*., 2011 and Li *et al.,* 2009). As a result, it is considered as an appropriate method for mechanical integrity studies of proton exchange membranes.

The use of pressure loaded blister/bulge testing for the characterisation of PEMs is attractive for several reasons. Due to the configuration of the test the preparation of the test specimens is simple and allows for simultaneous testing of multiple samples. The testing method is versatile in that apart from mechanical property data, it can be utilised to study permeation characteristics of the material as well as static fatigue and cyclic fatigue as a gaseous pressurisation medium is used (Li *et al.,* 2009). In addition, it is possible to utilise a liquid pressurisation medium, if the study requires a fully hydrated testing environment (Jai *et al.,* 2011). Because the system is scalable, it can be incorporated within an environmental chamber allowing for testing over an extensive range of environmental conditions found within electrochemical hydrogen energy systems (Merle, 2013). The use of an environmental chamber introduces a few additional advantages such as the possibility of hygrothermal cycling to impose stresses within the operational environment (Li *et al.,* 2009). It also allows the user to change the geometry of the specimen, while the frame in which the membrane is clamped eliminates grip failure associated with uniaxial tensile testing. Bulge/ blister testing is further a very attractive testing method due to the fact that it allows for a good representation of the environment found within electrochemical hydrogen energy systems as it mimics the stresses expected in the constrained membrane (Merle, 2013).

Through the implementation of bulge testing, it is possible to determine mechanical properties such as Young's modulus and residual stresses (Li *et al.,* 2009 and Merle, 2013). This is possible due to the correlation between the pressure and deflection of the specimen during testing. Schomburg (2011) developed mathematical equations to determine several membrane properties of thin membranes (d_M< 500 μm) based on Figure 2.2.

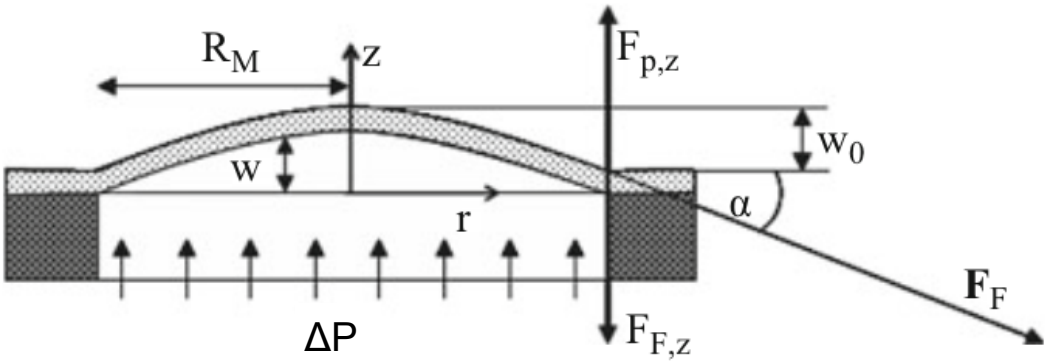

Figure 2.2. - Cross section of a pressure loaded circular thin membrane (Taken from Schomburg, 2011).

During pressurised blister testing/bulge testing the membrane loaded with a frame is subjected to a pressure change, resulting in a deflection of the membrane across the exposed area. This deflection results in strain across the matrix of the membrane generating stress. In the case where a circular membrane is clamped to prevent lateral movement when a constant pressure increase (ΔP) is applied, the deflection can be determined from the equilibrium forces at the rim. The total force, F_p (kN), acting on the membrane is equal to the product of the pressure difference and the exposed membrane area. This force is balanced by the force of the frame fixing the membrane to the circumference, F_F (kN). Because the membrane is fixed in a frame, there is no lateral movement during pressurisation and the lateral components of this cancel out when summed across the entire rim. The vertical components, $F_{p,z}$ (kN) and $F_{F,z,}$ (kN) of the applied pressure and the force of the frame respectively, are in equilibrium.

The product of the stress in the membrane during pressurisation, σ_M (MPa), and the cross-sectional area around the circumference, which is a product of the membrane thickness, d_M (mm), and the length circumference, $2\pi R_m$, gives the force of the frame. The vertical component can therefore be obtained by multiplying the force of the frame with the sine of the angle at which the membrane touches the frame. When the angle, α, is small, the sine is approximately the same as the slope of the membrane at the rim, which is equal to the tangent of α, and can be calculated as the derivative of the deflection curve at the rim.

$$F_{P,z} = \Delta P \pi R_M^2 = -F_{F,z} = -\sigma_M d_M 2\pi R_M \sin(\alpha) \qquad \text{(Eq.2.1)}$$

The curvature created during the pressurisation process can be described as the deflection curve of the membrane. Calculating the derivative of this and solving for the pressure drop results in:

$$\Delta P = \frac{4 w_0 d_M}{R_M^2} \sigma_M \qquad \text{(Eq.2.2)}$$

The stress, σ_M (MPa), of the membrane due to the applied pressure consists of three parts, the residual stress, σ_0 (MPa), which is present prior to any deflection of the membrane, the stress due to bending moments and the stress generated due to the stretching of the matrix.

$$\Delta P = \frac{4 d_M w_0}{R_M^2}\left(\frac{4}{3}\frac{d_M^2}{R_M^2}\frac{\mathrm{E}_M}{1-v_M^2} + \sigma_0 + \frac{64}{105}\frac{w_0^2}{R_M^2}\frac{\mathrm{E}_M}{1-v_M^2}\right) \quad \text{(Eq.2.3)}$$

The contributions of the bending moment and residual stress can be considered to be zero. This is a valid assumption as bending moments have little to no effect with the use of thin membranes, and as the membrane is clamped in a fixed position there is no initial residual stress (Schomburg, 2011, Li *et al.,* 2009 and Merle, 2013.). Therefore, Equation 2.3 can be rewritten as:

$$\Delta P = \frac{4 d_M w_0}{R_M^2}\left(\frac{64}{105}\frac{w_0^2}{R_M^2}\frac{\mathrm{E}_M}{1-v_M^2}\right) = \frac{4 d_M w_0}{R_M^2}\sigma_R \quad \text{(Eq.2.4)}$$

The radial strain is estimated by the extension of the membrane across its matrix, which is necessary for deflection. For thin membranes it can be assumed that the radial strain is constant over the entire membrane as bending moments do not occur. The length of the curvature during deflection can be calculated with Equation 2.5 based on Figure 2.4 if it is not measured using specialised equipment. Figure 2.3. - Length of a parabola as a result of deflection.

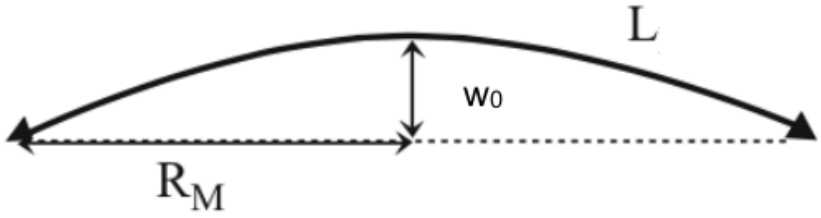

Figure 2.3. - Length of a parabola as a result of deflection.

A more detailed version of the above mentioned mathematical methodology behind bulge/blister testing as proposed by Schomburg (2011) is provided in Appendix A.

2.3. Viscoelastic properties of PFSA.

From Equation 2.4 it can be seen that by recording the pressure and deflection during bulge/blister testing it is possible to determine the Young's modulus and therefore the radial stress within the membrane specimen at the point of rupture. Throughout literature, examples of uniaxial tensile testing used for the determination of the Young's modulus of PFSA membranes have been recorded (Tang *et al*., 2006, Choi *et al.,* 2006 and Jia *et al.,* 2011). It is thus possible to find correlations between the pre-treatment, strain rate and environmental parameters in these studies.

Stress-strain behaviour at different temperature and RH has been investigated by Solasi *et al.* (2007). In this investigation the overall goal was to characterise the mechanical response of ionomer membranes in a constrained configuration whilst subjected to variable temperature and humidity environments. Uniaxial tensile testing was performed by fixing (50 mm × 6.5 mm) samples in a frame and exposing them to environmental changes in an environmental chamber with independent humidity and temperature control. All tests were conducted at a constant strain rate, although it was shown that the strain rate had no significant influence on the mechanical properties of the membrane. The authors reported that with an increase in water content the Young's modulus and yield stress of the membrane decreased. The same trend was observed for increasing temperatures, although it was suggested that temperature has a greater influence on the mechanical properties, yield stress in particular. During the study the Poisson's ratio was determined experimentally through video extensometry, and it was reported that a value of 0.4 was representative over the humidity ranges. All the above mentioned observations were confirmed in studies by Satterfield (2008), Li *et al*. (2009), and Grohs *et al.* (2010).

In Figure 2.4, presented by Satterfield (2008), it is observed that at low temperature, water reduces the Young's modulus of Nafion®, yet at high temperature water increases the Young's modulus. This observation once more confirms the observations made by Solasi *et al.* (2007).

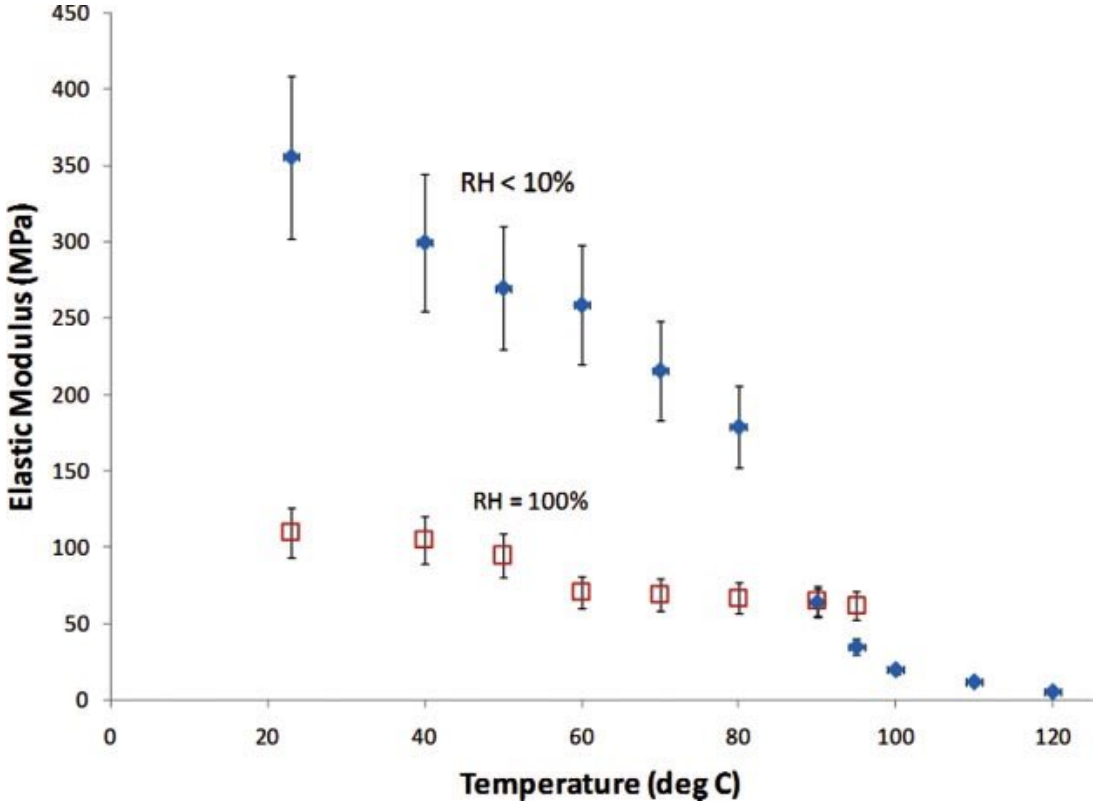

Figure 2.4. -Young's modulus of 1100 equivalent weight Nafion® as a function of temperature at 100% - <10% RH levels. (Taken from Satterfield, 2008).

Recently, work has expanded to cover a wider range of temperature and relative humidity combinations. Tang *et al.* (2006) investigated durability and degradation behaviour of Nafion® membranes under various mechanical, polarisation and chemical conditions. The authors used a custom environmental chamber, capable of controlling temperature and relative humidity, installed on a MTS Alliance RT/5 material testing system. Nafion® 112 was tested in 16 different environments: 25, 45, 65, 85 ℃ and 30 %, 50 %, 70 % and 90 % relative humidity with samples allowed 30 min to establish environmental equilibrium. The mechanical strength of the membranes was measured at a constant strain rate of 0.2 mm/min with an initial gauge length of 50 mm. The authors reported results for Young's modulus, ultimate stress and strain and the yield stress and strain. Additionally, the authors investigated the mechanically induced stress due to temperature and humidity cycling. For this phase the membrane samples were loaded in a single cell and subjected to up to 1000 cycles at different stress levels (One cycle is equal to 8 min at high RH and 2 min at low RH) at 90 ℃. It was found that the PEM was stable under a cyclic stress of up to 1.5 MPa. At 3.0 MPa, the dimension of the membrane changed significantly and physical breakdown was visible. At 6.5 MPa, many cracks appeared on the surface of the membrane indicating rupture of the membranes' microstructures. The results of Tang *et al.* (2007) agree with previous findings that increased water content and temperature decrease membrane stiffness. Similar observations were made by Li *et al.* (2010) and Shi *et al.* (2013).

As proton exchange membranes are becoming a better understood commodity, the field of research has expanded over the last decade. In the pursuit of making the membranes more durable, much work has been devoted to the degradation of the membranes. It has been observed that mechanical degradation of PEMs is a common failure mechanism which is largely caused by contamination (Jia *et al.,* 2011). Contamination may be introduced by impure reactant gases, corrosion of components in the gas distribution system such as tubing or fitting materials as well as ions in the water supply which result in cation exchange in the PEM causing deterioration of the fuel cell performance (Jia *et al.,* 2012 and Kundu *et al.,* 2005).

The effect of contamination related to cation exchange on the mechanical reliability of PEMs was investigated by Jai *et al.* (2011). The authors used a bulge testing method with water as pressure medium to characterise the biaxial stress-strain behaviour of the membranes under fully hydrated conditions. The effect of cation contamination was assessed by comparing the elastic deformation of Nafion® 211 membranes as received (H^+-form) to that of Nafion® 211 membranes exposed to Fe^{3+}, Mg^{2+}, Cu^{2+}, Li^+, Na^+ and K^+ contaminants.

To conduct the bulge test deionised water (DIW) was used as medium to simulate the hydrated pressure loading on the PEM in fuel cells. A syringe plunger was used to control the pressure, measured with a pressure transducer, within the system. Nafion® samples were then clamped to the setup, touching the water medium for a 10 min period. The system was positioned inside an environmental chamber with the experiments carried out at a constant relative humidity (25% RH) and temperatures of 23 ℃ and 80 ℃ simulating operational conditions of functional fuel cells. The bulge height was measured using an optical microscope.

In addition to the bulge testing, Jia *et al.* (2011) also investigated the elastic moduli of the membranes through uniaxial testing. The uniaxial testing was conducted with a mechanical testing system at combinations of two different relative humidities (25 % and 100 %) and temperatures 23 ℃ and 80 ℃. The samples (10 mm × 80 mm) were pre-treated for a 30 min period at the specific conditions and then loaded in tension at a constant crosshead speed of 0.1 $mm.s^{-1}$.

Using data obtained from applied pressure and bulge height, the biaxial stress of the ion exchanged species were determined and compared to that of non-contaminated samples. It was observed that stiffness of elastic deformation increased with the addition of metal ions in the order of H^+, Li^+, Na^+ and K^+ corresponding to results published by Kawano *et al.* (2002) and Kundu *et al.* (2005). Jia *et al.* (2011) reported that the Young's modulus determined for completely hydrated samples was considerably lower than that of samples at 25 % RH. It was further concluded that the reduction of the Young's modulus was a result of plasticisation of the PFSA polymer by water absorption.

The Young's modulus of the contaminated specimens was observed to increase with increasing radius of the cation used for contamination, which was explained by the cations' affinity to the sulfonic acid groups in the PFSA molecules. The larger cations interact with more sulfonic acid groups thereby reducing the mobility of the side chains, leading to increased stiffness of the membrane. Kundu *et al.* (2005) observed a similar phenomenon by uniaxial tensile tests in salt solutions. It was suggested that the limited surface area of cations prevent further physical cross linking amongst side chains of the PFSA molecules despite higher charge densities of multivalent cations. In addition, it was mentioned that the water content could be affected differently by the different cations, thereby influencing the elastic moduli (Jai *et al.,* 2011). Because the foreign cations have larger radii than the original H^+-ion, less water is absorbed in the membrane, reducing the effect of water content on the weakening ionic interactions. This reduction of water content decrease the mobility of the side chains, lowering the flexibility of the molecules around the cluster, causing the stiffness of the membrane to increase (Collier *et al.,* 2006 and Jai *et al.,* 2012). This theory is schematically shown in Figure 2.5.

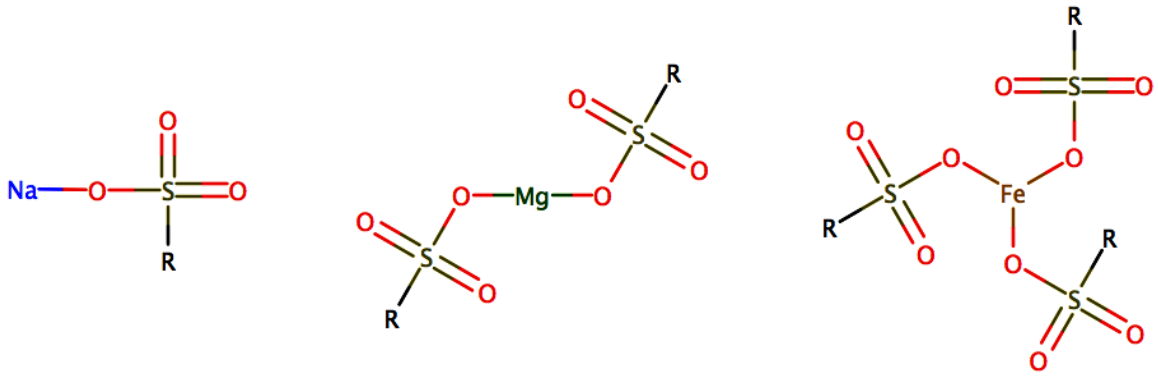

Figure 2.5.- Schematic representation of cation impurities occupying sulfonic acid groups in the Nafion® structure.

*R is defined in Figure 2.1.1.

A review on the elastic moduli of Nafion® was given by Satterfield (2008) with results up to the year 2005, while any work post 2005 was summarised by the author. The summary of data is presented in Table 2.1 which includes results from the case studies discussed above. Note that values read from published curves are indicated with the ~sign.

Table 2.1 - Summary: Young's modulus of Nafion®.

Researcher, Year	Material	Apparatus	Method	Water Content	Temp	Young's modulus [MPa]
DuPont product information	Nafion® PFSA membranes, N-112, NE-1135, N-115, N-117, NE-1110		ASTM D 882	50% RH	23℃	249
				water soaked	23℃	114
					100℃	64
Werner, Jorissen *et al.*, 1996	Nafion® 117, 50mm length	Zwick 1445 Universalpruf-maschine	Strain rate: 0.2/min in machine direction	Dry	25℃	~100
				"Completely humidified"	25℃	~50
				Unspecified	200℃	~1
Kwano, Wang *et al.,* 2002	Nafion® 117, Aldrich, acid form, 25mm length×6mm	T.A Instruments DMA 2980, controlled force mode, tension	Preload force: 0.005N, soak time: 1min, force ramp rate: 0.5N/min, upper force: 18.0N	water soaked, 24h	27℃	95
				boiling water soaked, 1h	27℃	128
				as-received	27℃	200
					60℃	147
					90℃	44
					120℃	5
					150℃	3
					180℃	2
				dry: vacuum oven 70℃, 24h	27℃	210
					60℃	176
					90℃	80
					120℃	13
					150℃	4
					180℃	2
Kundu, Simon *et al.,* 2005	Solution cast Nafion® 117, 5mm gauge length×6mm	Rheometrics DMTA V, tension	Preload force:0.1N, strain rate: 0.001/min, max strain: 0.015-0.024	water soaked	80℃	~45
	Solution cast Nafion® 112					~35
Fujimoto, Hicknet *et al.,* 2005	Nafion® 117, 30mm gauge length×9mm	Com-ten Industries 95T series load frame equipped, load cell:200 lbf	Strain rate: 0.17/min	Ambient	RT	200
				soaked in water until tested	RT	52

Researcher, Year	Material	Apparatus	Method	Water Content	Temp	Young's modulus [MPa]
Kyriakides 2005; Liu, Kyriakides *et al.,* 2006	Nafion® 117: pre-treated boiling 0.5M H_2SO_4 2h & boiling DI water 2h, dried 70℃ vacuum, 40mm gauge length×12mm	Instron 4468 screw-driven universal testing machine, load cell: 1kN	Strain rate: 0.7/min	equilibrated at 23℃, 40%RH 72h, water concentration: 5.3±1.5%	23℃	270 ± 4
			Strain rate: 0.3/min			253 ± 7
			Strain rate: 0.12/min			256 ± 18
			Strain rate: 0.07/min			263 ± 10
			Strain rate: 0.025/ min			250 ± 5
Tang *et al.,* 2006	Nafion® 112: pre treated boiling 3%H_2O_2, 0.5M H_2SO_4 and DI 1hr, 50mm gauge length×10mm	MTS Alliance RT/5 material testing system	Strain rate: 0.2/min	30% RH	25℃	~230
				50% RH		~180
				70% RH		~150
				90% RH		~110
				30% RH	45℃	~170
				50% RH		~147
				70% RH		~122
				90% RH		~80
				30% RH	65℃	~127
				50% RH		~110
				70% RH		~90
				90% RH		~70
				30% RH	85℃	~83
				50% RH		~75
				70% RH		~60
				90% RH		~45
Choi *ei al.,* 2006	Nafion® 112	Thermal analysis 2980 DMA instrument	OEH Technique	10% RH	40℃	~280
				40% RH		~240
				60% RH		~210
				90% RH		~190
				10% RH	60℃	~245
				40% RH		~210
				60% RH		~190
				90% RH		~160
				10% RH	80℃	~120
				40% RH		~100
				60% RH		~90
				90% RH		~80

Researcher, Year	Material	Apparatus	Method	Water Content	Temp	Young's modulus [MPa]
Jia *et al.,* 2011	Nafion® 211: pre treated 30 min exposure to environment, 80mm gauge length × 10 mm	MTS 810, MTS systems corporation, Eden Prairie, MN	Strain rate: 0.1/min Nafion®-H^+	25% RH	23℃	283
				100% RH		101
				25% RH	80℃	178
				100% RH		95
			Strain rate: 0.1/min Nafion®-Li^+	25% RH	23℃	373
				100% RH		111
				25% RH	80℃	351
				100% RH		103
			Strain rate: 0.1/min Nafion®-Mg^{2+}	25% RH	23℃	375
				100% RH		138
				25% RH	80℃	381
				100% RH		124
			Strain rate: 0.1/min Nafion®-Fe^{3+}	25% RH	23℃	334
				100% RH		175
				25% RH	80℃	322
				100% RH		96
Moukheiber *et al.,* 2014	Aquivion E110	ADAMELL homargy tensile machine	Strain rate: 0.5/min, 50mm gauge length× 20mm	60% RH	25℃	127 ± 7
	Nafion® 111					110 ± 20
	Nafion® XL100					126 ± 14

2.3.1. Review summary

From the main findings in the review it can be concluded that the Young's modulus of Nafion® is dependent on several variables like preconditioning, method of humidification, time allowed for equilibrium to be reached, humidification temperature, strain rate and environmental conditions during testing.

From the results of Tang *et al.* (2006) and Choi *et al.* (2006) it is clearly seen that the Young's modulus is influenced by the preconditioning of the membrane. For example a sample pre-treated in H_2O_2 by Tang *et al.,* 2006 prior to testing at 90 % RH and 45 ℃ had a Young's modulus of 80 MPa, while a sample tested at 90 % RH and 40 ℃ had a Young's modulus of 190 MPa. However, pre-treatment with H_2SO_4 by Kyriakides *et al.* (2005) showed nearly no impact compared to the untreated samples. It is therefore clear that the chemicals used for pre-treatment should be chosen wisely, as it can negatively influence the viscoelastic properties of the materials.

The Young's modulus of the membranes tends to decrease as temperatures and RH increase as seen from most sources. Further it appears that the Young's modulus is lower when the specimen is soaked in water compared to when it is humidified by water vapour. For example DuPont (2015) reported a Young's modulus of 114 MPa and 249 MPa for water soaked and vapour humidification respectively at 23 ℃. This can be contributed to the fact that liquid water is a better source of humidification, therefore more water is absorbed lowering the Young's modulus. A reduction of the Young's modulus is also observed with an increase in the humidification temperature, whereas it seems that an increase in strain rate negatively impacts the Young's modulus as well, although the impact is minimal.

Work published on cation exchange within PEMs revealed that the size and valence of the ion influences the water uptake of the material. It was concluded that the presence of cations reduces water uptake, thereby increasing the stiffness of the membrane, causing an increase of the Young's modulus.

Additionally, several assumptions were commonly made throughout the reviewed literature *e.g.* Poisson's ratio can be accepted as 0.4 for Nafion®, a period of 30 min is sufficient time for the membrane sample to reach equilibrium with the surrounding environment and a period of 48 hours is sufficient time for complete ion exchange to occur when excess cations are available in the solution.

Chapter 3 - Experimental

An introduction to different PEM materials and how their viscoelastic and mechanical properties can be determined was given in Chapter 2. It was indicated why the primarily focus is placed on Nafion® membranes and why bulge/blister testing is the preferred method for the investigation of the viscoelastic properties. Specifications on the method used for the determination of the biaxial strength and behaviour of these membranes under different environmental conditions were also provided. Trends of the Young's modulus as determined through uniaxial tensile testing under different environmental conditions were also discussed to give some perspective on what is expected from this study. Details of the experimental setup, materials and experimental procedures are given in Chapter 3. In Section 3.1 the materials used during experimental procedures are listed. The equipment used in the experimental rig and experimental procedures are discussed in Section 3.2 and Section 3.3 respectively.

3.1. Materials

The membrane samples tested in this study were DuPont™ Nafion® NR 115, Nafion® NR117 and Nafion® NR 1110 perfluorosulfonic acid (PFSA) membranes that were supplied by Ion Power (New Castle, Unites States). In addition, reinforced membranes supplied by Fumatech® (Ludwigsburg, Germany) and a non-disclosed original equipment manufacturers (OEM) and non-hydrolysed perfluorinated membranes in the sulfonyl fluoride form, supplied by PlastPolymer (St. Petersburg, Russia) were tested for comparative analysis between non-reinforced Nafion® membranes.

The gas used as pressurisation medium during rupture testing was nitrogen supplied by Afrox (Potchefstroom, South Africa). Chemicals used for the contamination and hydrolysis process of membrane samples in different experimental procedures were: sodium chloride (NaCl), magnesium chloride hexahydrate ($MgCl_2 \cdot 6H_2O$), iron (III) chloride hexahydrate ($FeCl_3 \cdot 6H_2O$), sodium hydroxide (NaOH) and hydrochloric acid (HCl) all provided by Sigma Aldrich (St. Louis, Missouri, United States). The material safety data sheets (MSDS) are provided digitally on the enclosed CD/USB (Materials/MSDS). A list of materials used in the experimental procedures as well as Nafion® material specifications as provided by the supplier are provided in Table 3.1 and Table 3.2 respectively.

Table 3.1 - List of materials and suppliers.

Material	Supplier	Purity	Reference name
Nafion® 115	Ion Power		NR115
Nafion® 117	Ion Power		NR117
Nafion® 1110	Ion Power		NR1110
Reinforced membrane 1	Fumatech		Fumatech
Reinforced membrane 2	Non disclosed OEM		OEM1
Non-hydrolysed perfluorinated membranes	PlastPolymer		PlastPolymer
Compressed Nitrogen gas	Afrox	≥ 99.99%	N_2
Sodium chloride	Sigma-Aldrich	≥ 99%	NaCl
Magnesium chloride crystal	Sigma-Aldrich	≥ 99%	$MgCl_2 \cdot 6H_2O$
Iron(III) chloride hexahydrate	Sigma-Aldrich	≥ 96%	$FeCl_3 \cdot 6H_2O$
Sodium hydroxide (NaOH)	Sigma-Aldrich	≥ 97%	NaOH
Hydrochloric acid (HCl)	Sigma-Aldrich	33.6 wt%	HCl

Table 3.2 - Properties of Nafion® Perfluorosulfonic Acid Membranes as supplied by DuPont (2015).

Nafion® Type	Thickness (μm)	EW (g.meq^{-1})	Basis weight (g/m^2)
NR115 (extruded)	130	1100	250
NR117 (extruded)	180	1100	360
NR1110 (extruded)	240	1100	500
Property	**NR115, 117, 1110**		
Tensile modulus, 50% RH (MPa)	249		
In 23°C water	114		
In 100°C water	64		
Maximum tensile strength, 50% RH (MPa)	43 MD, 32 TD		
In 23°C water	34 MD, 26 TD		
In 100°C water	25 MD, 24 TD		
Elongation at break, (%) 50% RH	225 MD, 310 TD		
In 23°C water	200 MD, 275 TD		
In 100°C water	180 MD, 240 TD		
Tear Resistance, initial (g/mm) 50% RH	6000 MD & TD		
In 23°C water	3500 MD & TD		
In 100°C water	3000 MD & TD		
Tear Resistance, propagation (g/mm) 50% RH	>100 MD, >150 TD		
In 23°C water	92 MD, 104 TD		
In 100°C water	74 MD, 85 TD		
Water uptake at 100°C (%)	38		
Linear Expansion in 100°C water, (%)	15		

*Machine direction (MD) and transverse direction (TD) refers to two different methods used for determining the material properties.

3.2. Equipment

3.2.1. Uniaxial tensile testing

A MTS Criterion C45.503 Universal Tensile Tester (UTT) was used in accordance with an extensometer, for increased accuracy, to perform uniaxial tensile stress tests at IMP Calibration Services™ (Germiston, South Africa). An image of the machinery is shown in Figure 3.1.

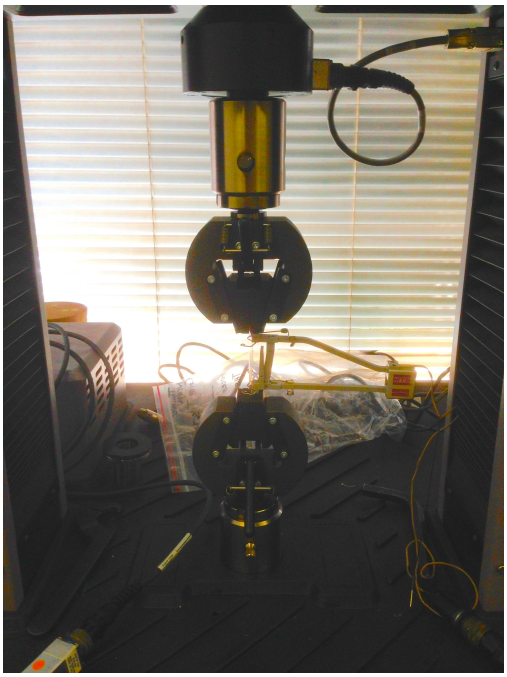

Figure 3.1. - MTS Criterion C45.503 Universal Tensile Tester used for uniaxial testing.

3.2.2. Biaxial tensile testing

A high pressure gas rupture test was designed and manufactured in house on the basis of pressurised bulge/blister testing to conduct biaxial tensile testing. The concept of loading a thin membrane specimen using a pressure-loaded blister test was illustrated in Figure 2.2, in which it showed the specimen clamped around the edge and allowed to deflect into a blister/bulge through a circular opening with radius R_M, when loaded with pressure from one side. The radius at the front side of the stainless steel (SS) cell and the PTFE O-rings were both 20 mm, but was changeable by placing a stainless steel plate inside the cell, reducing the diameter to 15 mm or 10 mm, whilst the 20 mm O-rings were replaced with new ring sizes as determined by the plate placed in the cell. Pressurised nitrogen was fed to the system to pressurise the specimen. The PTFE O-rings along with the large gripping area were included to enhance the gripping of membrane samples. A three-dimensional drawing of the design of the high-pressure cell is provided in Appendix B.

A schematic of the experimental system used in the determination of the mechanical stability of the proton exchange membranes is presented in Figure 3.2. Baseline nitrogen gas (Afrox) was supplied to the system at bottle pressure of 100 - 200 barg while the system pressure was controlled by a front pressure regulator (P-REG). Electrically actuated solenoid valves (SV1 & SV2) were included to control the flow of gas to the system and as an added safety feature. The pressure supply of the system was monitored by a pressure transducer (P1) while another pressure transducer (P2) monitored the pressure supplied to the membrane. Two safety relief valves (PRV1 and PRV2) ensured that no overpressure (> 200 barg) was possible. A needle valve (NV1) was used to control the N_2 flowrate to the high-pressure cell. A second needle valve (NV2) was used as a relief valve, to purge any gas remaining in the system after testing. After the membrane sample was secured and fastened in the high-pressure cell, it was connected to the rest of the system via a connection that introduced the environmental chamber (ESPEC SH-221), which controlled both the temperature and humidity. The pressure cell was designed in such a way that the membrane was exposed to the humidified atmosphere. An additional pressure sensor (P3) was included as a safety feature in case P2 failed. The system was controlled using Labview®. A thermal mass flow meter (FLOW) was included in the system to support requirements for future testing using the system. As the flowrate of N_2 was not a required parameter in the current scope FLOW was placed beyond NV2 to keep the system as minimalistic as possible. However, the flowrate could be determined by sealing the pressure cell and allowing the N_2 to flow through the system. From Figure 3.3 it can be seen that the membrane sample was exposed to the controlled environment on one side while the other side was exposed to the high pressure. An image of the gas feed system is presented in Figure 3.4. The equipment schedule is provided in Appendix C and the safety equipment and laboratory rules are discussed in Appendix D.

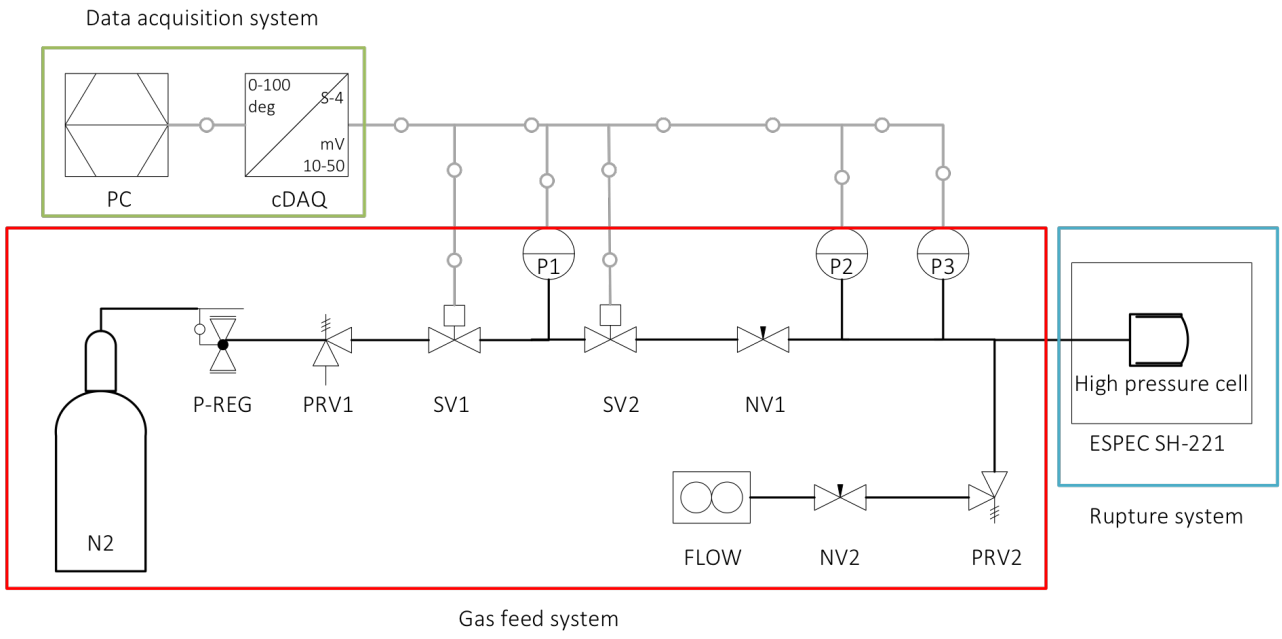

Figure 3.2 - Schematic of experimental setup.

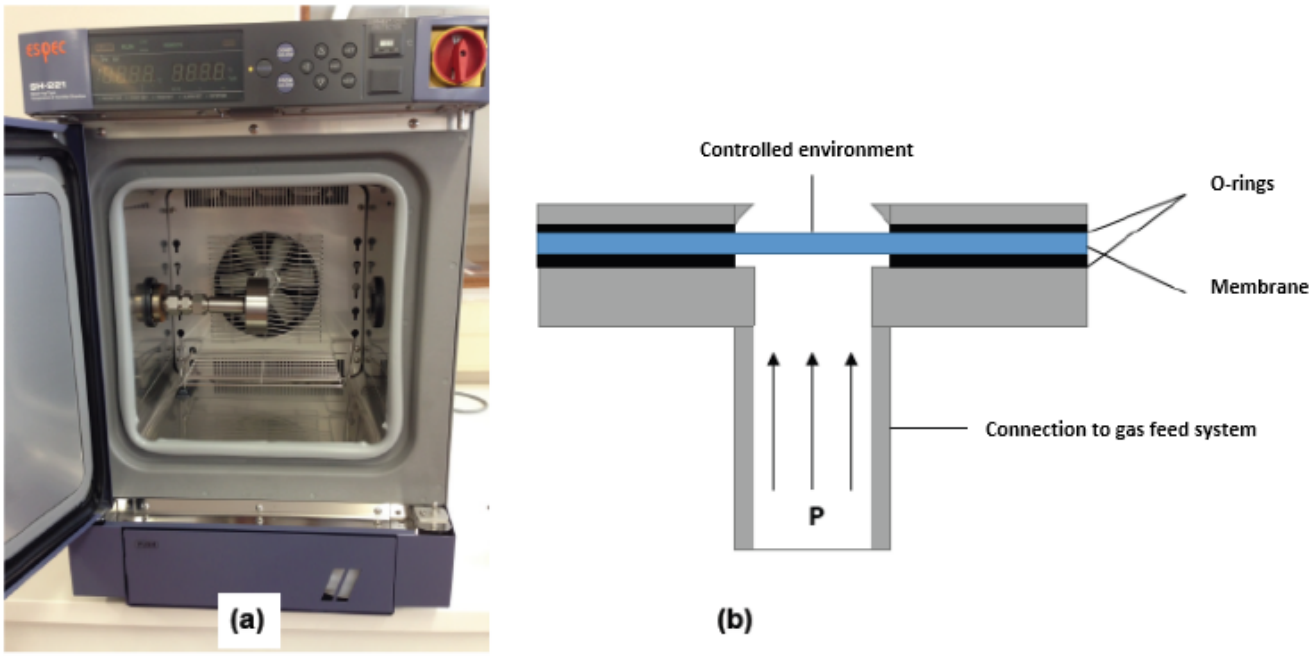

Figure 3.3 - (a) High-pressure cell inside environmental chamber (b) Schematic representation of high-pressure cell construction.

Figure 3.4 - Generation 1 high-pressure membrane rupture test rig..

3.3. Procedures

3.3.1. - Uniaxial tensile testing

A MTS Criterion C45.503 Universal Tensile Tester (UTT) was used to perform uniaxial tensile stress tests. Membrane samples with an average length to width ratio of six to one were used. The membrane samples were 20 mm in width and 120 mm in length. The edges of the specimen were then clamped in the UTT machine with a gauge length of 50 mm.

To conduct tests at various relative humidity levels, an ESPEC SH221 environmental chamber was used to condition the membranes. The test samples were first dried for 24 hours at 60 ℃ to ensure that the specimens were free of moisture prior to testing. The membrane samples were pre-conditioned in the environmental chamber for a 30 minute period to allow the sample sufficient time to reach thermal and moisture equilibrium (Jia *et al.* 2011).

The approach taken for acquiring uniaxial tensile stress data was to test the membrane sample at a given temperature over a range of relative humidity levels of 35 %-90 % in 20 % intervals. A new specimen was used for each increment in relative humidity. The tests were conducted at 20 ℃, as it was the only temperature in the desired range that was completely controllable outside the environmental chamber. The typical test duration was 15 minutes with a set strain rate of 5 mm/ min for each test.

The test was considered complete at the point that the specimen broke, after which the clamps were opened and the gauges reset for the following specimen. For each new humidity test, the sample length was automatically reset by the machine prior to applying any strain. The Young's modulus was obtained by determining the initial slope of the load vs strain curve. A load vs strain curve was compiled for each membrane type at 20 ℃ at a relative humidity level of 35 %, 50 %, 70 % and 90 %, from which the Young's modulus was calculated for each sample respectively.

3.3.2. Biaxial tensile testing

In the biaxial tensile testing a membrane specimen of 56 mm diameter was cut from a flat sheet of the material. The specimen was the dried in an ESPEC-SH221 environmental chamber at 60 ℃ for a 24 hour period for moisture removal. The specimen was then placed in between the two O-rings, placed in the high-pressure cell and provided with a gas tight seal using gas-tight PTFE tape. After securing the membrane sample in the high pressure cell, it was connected to the gas feed system, while inside the environmental chamber. The membrane sample was left for 30 min at the desired environmental condition of temperature (varying between -15 ℃ and 80 ℃) and RH (varying between 35 % and 90 %) before commencing the pressure increase. The 30 min exposure time was chosen as it was deemed sufficient time to reach equilibrium as in previous studies (Tang *et al.,* 2007 and Jia *et al.,* 2011).

The SV1 and SV2 were opened, allowing the system pressure to gradually increase until complete rupture of the membrane in the high-pressure cell was achieved. The pressure was measured digitally every second. The strain rate observed was 5 mm/min which was in accordance with the strain rate during uniaxial tensile testing. The deflection of the membrane during pressurisation was measured using two different methods. The first of which was visually, through the use of a webcam (Logitech) during operation and the second was by measuring the distance across the curvature at the point just prior to rupture. With regards to the first method, a webcam was placed inside the environmental chamber, and a video was recorded of the rupture test. Thereafter, the video was analysed and the deflection was measured by hand. An example of this method is included on the accompanied CD/USB (Experimental procedure/Rupture test) and can also be viewed online at http://www.hysainfrastructure.org/?p=3375 . Alternatively, a string was used to measure the distance across the centre of the formed curvature at the moment before rupture, and using Equation 2.5, the deflection was calculated. The deflection of NR115 at 20 ℃ and 35 % RH was measured as 4.35 mm and 4.31 mm using the webcam and string method respectively. These deflections were equivalent to rupture pressures of 0.506 MPa and 0.519 MPa respectively, showing that the two methods do not differ significantly. Details on the comparison of the two methods are provided in Appendix E. The visual method was used throughout the experimentation.

The deflection (w_0) and pressure (P) were recorded during the experimental procedures enabling the calculation of the Young's modulus with Equation 2.4. The experimental method was validated by comparing the data recorded from biaxial tensile testing to the results obtained through uniaxial tensile testing which is discussed in Section 4.1.

3.3.3. Contamination of Nafion® membranes

In the investigation of the effect of metal ion contamination on the Young's modulus and rupture pressure of the membrane specimens, a circular NR1110 sample of diameter 56 mm, was boiled in a 100 ml saturated solution of NaCl, $MgCl_2 \cdot 6H_2O$ and $FeCl_3 \cdot 6H_2O$ respectively for a 48 hour period. The 48 hour period was regarded as a sufficient period to establish complete ion exchange (Jia *et al*., *2011)*. By placing the membrane in a saturated solution of the respective chemicals, the H^+ ions of the sulfonic acid groups of the membranes were completely exchanged with Na^+, Mg^{2+} and Fe^{3+} ions respectively. The specimens were removed from the solutions, and dried for 24 hours at 60℃. The contaminated specimen, in metal-ion form was then subjected to the rupture test for the determination of the rupture pressure and Young's modulus.

3.3.4. Partially hydrolysed membranes

Non-hydrolysed perfluorinated membranes were prepared from a flat sheet. The membrane samples were partially hydrolysed by boiling them in a solution of 6 M NaOH at 80 ℃ (Bessarabov *et al.* 2000) for 30 min, 60 min, 5 hrs and 24 hrs respectively. The membranes were washed with

distilled water and placed in distilled water at a temperature of 100℃ for 30 minutes. The hydrolysis reaction of a non-hydrolysed membrane can be expressed as:

$$R-SO_2F \xrightarrow[-HF]{NaOH/H_2O} R-SO_3Na+NaF \qquad \text{(Eq. 3.1)}$$

where R is a general description of a perfluorinated polymeric matrix.

The various partially hydrolysed membranes (in Na^+ ionic form) were then placed in separate 40 ml solutions of 0.1 M HCl for 12 hours to protonate the membrane. The number of moles of Na^+ ions that was subsequently exchanged with H^+ ions was then determined by back titration. Samples (5 ml) of the HCl solution used for ion exchange were titrated with 0.1 M NaOH, using phenolphthalein as indicator, to determine the concentration of the HCl solution after the ion-exchange process (Bessarabov *et al.*, 2000). The ion exchange capacity (IEC) and equivalent weight (EW) of the hydrolysed membranes were calculated with Equation 3.2 and Equation 3.3.

$$IEC = \frac{N_{st}\left(\frac{V_{HCl}-V_{NaOH}}{V_{HCl}}\right)\times V_{IE}}{M_{membrane}} \qquad \text{(Eq. 3.2)}$$

$$EW = \frac{1000}{IEC} \qquad \text{(Eq. 3.3)}$$

The membranes were removed from the 40 ml solutions after protonation, dried for 24 hours at 60℃ and tested.

Chapter 4 - Results and Discussion

The literature overview provided in Chapter 2 gave an introduction to different PEM materials, bulge/blister testing and how the mechanical and viscoelastic properties of PEMs can be determined. Details of the experimental setup, materials and experimental procedures were given in Chapter 3. The results recorded during experimental procedures are provided and discussed in Chapter 4. In Section 4.1 uniaxial tensile testing and biaxial tensile testing are compared to each other and the validity of the method proposed by Schomburg (2011) is investigated. The viscoelastic and mechanical properties of PEMs, as determined through biaxial tensile testing is discussed in Section 4.2. Section 4.2.1 will focus on the effect of temperature and RH on the viscoelastic properties of PEMs. Additional parameters influencing the viscoelastic and mechanical properties of the tested materials, such as sub-zero temperatures (Section 4.2.2), cation contamination (Section 4.2.3), membrane reinforcement (Section 4.2.4) and partially hydrolysed membranes (section 4.2.5), are then discussed. It will be shown that membrane thickness has little to no influence on the Young's modulus (at the same conditions) while an increase in RH, temperature reduces the Young's modulus whilst cation contamination increases the Young's modulus.

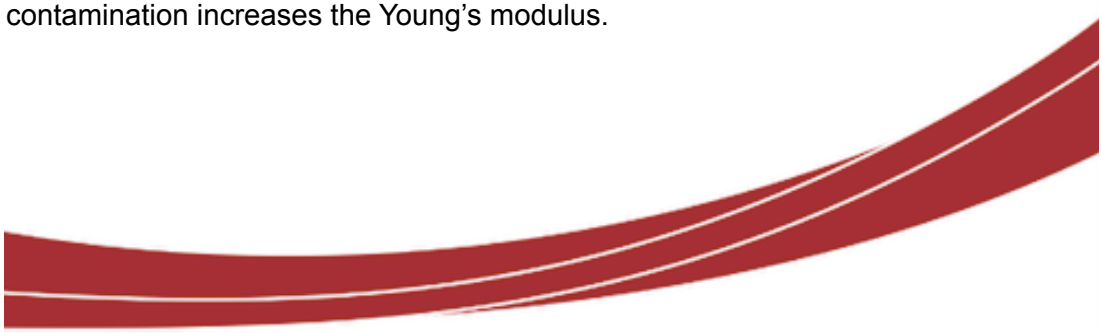

4.1. Validation of biaxial tensile testing as a method for the characterisation of proton exchange membranes

The results from uniaxial tensile testing of a NR115 membrane specimen at 20 ℃ and 35 % RH are presented in Figure 4.1. The Young's modulus is determined from the initial slope of the load vs strain plot, using Equation 4.1. Although two distinct regions are observed, only the first region is of importance for the determination of the Young's modulus, whereas the second region will typically be used in to calculate the stress at breakpoint of less elastic materials such as steel.

$$E \equiv \frac{\sigma}{\varepsilon} = \frac{F / A_0}{\Delta L_T / L_0} = \frac{F L_0}{A_0 \Delta L_T} \qquad \text{(Eq. 4.1)}$$

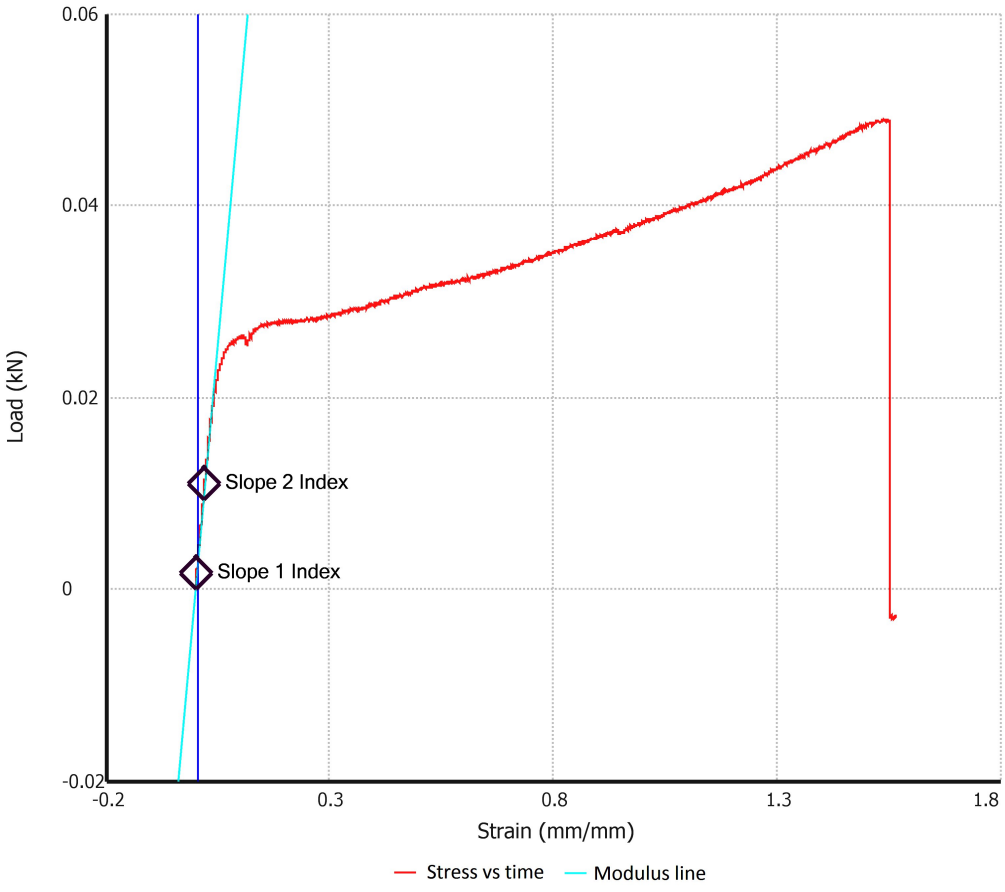

Figure 4.1 - Load vs Strain of NR115 at 20 ℃ and 35 % relative humidity during uniaxial tensile testing.

A summary of the results obtained from the uniaxial tensile testing on NR115, NR117 and NR1110 samples at 20 ℃ and 35 %, 50 %, 70 % and 90 % RH is presented in Table 4.1.

Table 4.1 - Young's modulus of Nafion® membranes determined through uniaxial tensile testing over a relative humidity range of 35 % to 90 % at 20 ℃.

Young's modulus (MPa)			
Relative humidity (%)	**NR 115 (130μm)**	**NR 117 (180μm)**	**NR 1110 (240μm)**
35%	196		195
50%	167	168	169
70%	141	146	
90%	133	135	130

*Vacancies within Table 4.1.are due to grip failure during testing, resulting in inconclusive data.

From this table it can be observed that the Young's modulus remains constant for each of the various membrane samples at a specific environmental condition, and it is therefore concluded that the property is not dependent on membrane thickness. The consistency of the values can be contributed to the chemical and thermal stability of the Nafion® membranes when all pre-treatment and testing parameters are controlled. Therefore, the Young's modulus of Nafion® materials with the same EW remains constant at a specific environmental state. As a result it is possible to determine the viscoelastic properties of one membrane thickness and interpret the results as representative of any membrane thickness with the same EW.

A statistical regression analysis was conducted to determine the experimental error of the high-pressure rupture test rig used for the biaxial tensile testing. The experimental error was determined as 6 %, which is comparable to the 5 % experimental error of the UTT (as provided by IMP Calibration Services™) used for uniaxial tensile testing. The statistical regression analysis is presented in Appendix F. Biaxial tensile testing was conducted on the same membrane specimens used during uniaxial tensile testing to evaluate the Young's modulus values obtained through the two methods respectively. The Young's modulus was determined for each membrane as a function of RH at 20 ℃. The values obtained through biaxial- and uniaxial tensile testing are compared in Figure 4.2.

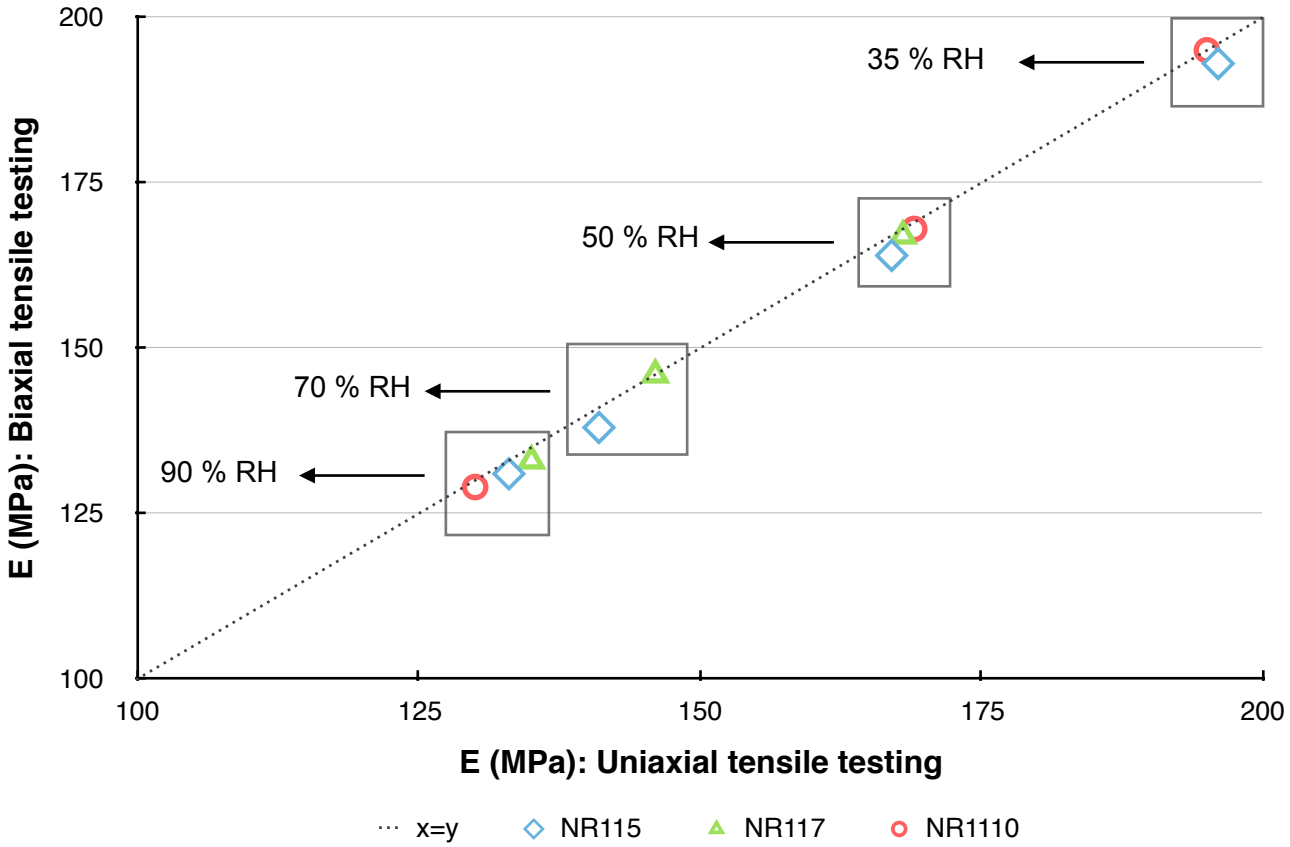

Figure 4.2 - Comparison of Young's modulus of Nafion® membranes at 20 ℃ obtained through uniaxial- and biaxial tensile testing.

*Henceforth, it should be noted that solid lines represent a model and dotted lines are used to guide the readers to observe trends in data presented by markers.

From Figure 4.2 it is seen that the values obtained by biaxial tensile testing do not differ significantly from the values obtained by uniaxial tensile testing. On average, the values from the biaxial tensile testing method are 1.3 % lower than that obtained by the conventional method, which serves as validation that the method used for the biaxial tensile testing can be used with confidence as it is accurate and comparable to uniaxial tensile testing.

The validity of the model proposed by Schomburg (2011) in Equation 2.4, was evaluated as a function of RH at 20℃. A single value for the Young's modulus was fitted to the model to construct a theoretical line of the deflection as a function of pressure. The experimental videos were analysed after the biaxial tensile testing, and deflection and corresponding pressures were plotted against the model to evaluate the correlation between the model and the data. The results are presented in Figure 4.3.

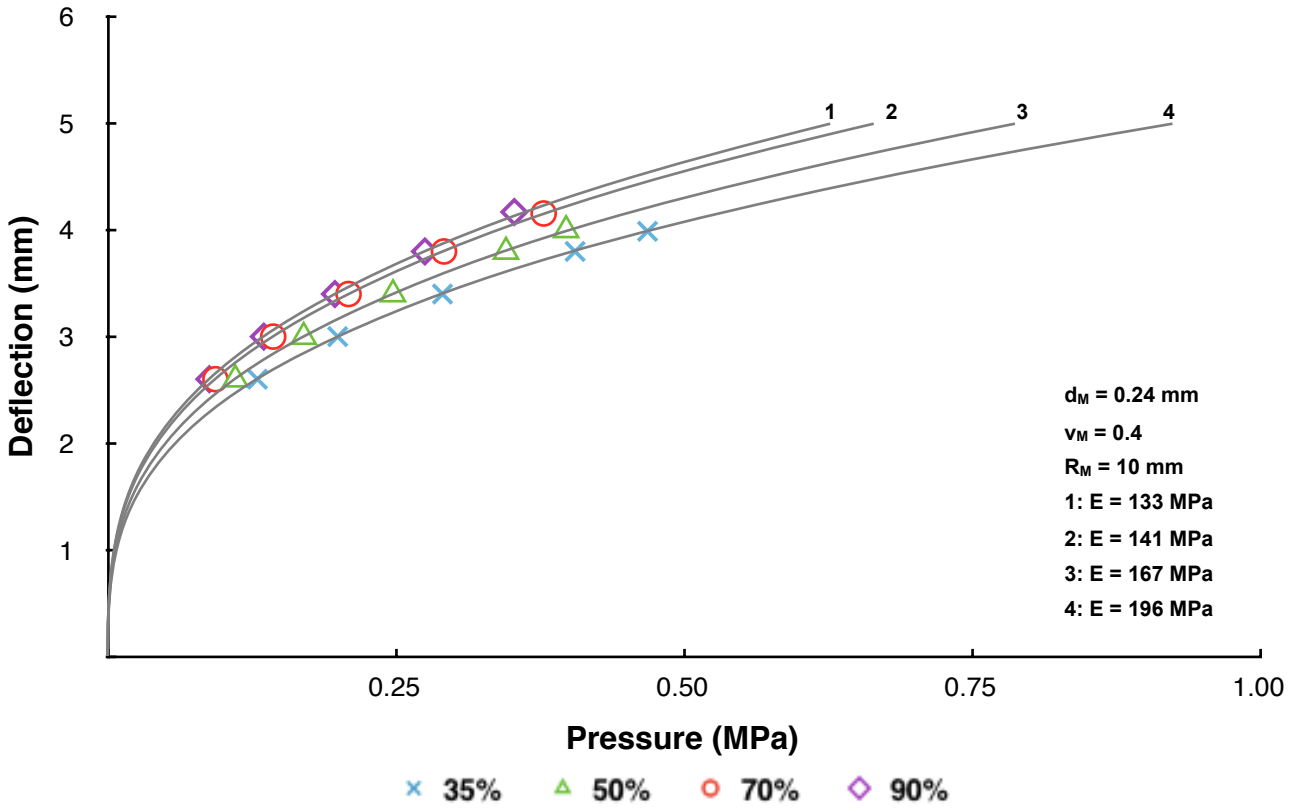

Figure 4.3 - Comparison of Young's modulus of NR115 determined theoretically through the model proposed by Schomburg (2011) and biaxial tensile testing at 20 ℃.

From Figure 4.3 it is observed that for each condition, where one fixed value is used for E with Equation 2.4, the model proposed by Schomburg (2011) is valid throughout the experiment. The Young's modulus can thus be determined accurately at any point during biaxial tensile test with the measurement of the deflection and the subsequent pressure.

The model was further used to investigate the effect of the sample radius on the Young's modulus. The radius of the blister area was varied to 5 mm, 7.5 mm and 10 mm, and the biaxial tensile testing was conducted at 50 % RH and 50 ℃. A model line was constructed for a Young's modulus value of 106 MPa for each of the different radii. The deflection and corresponding pressure at selected points were recorded and plotted against the theoretical values to further evaluate the accuracy of the model. The results are presented in Figure 4.4.

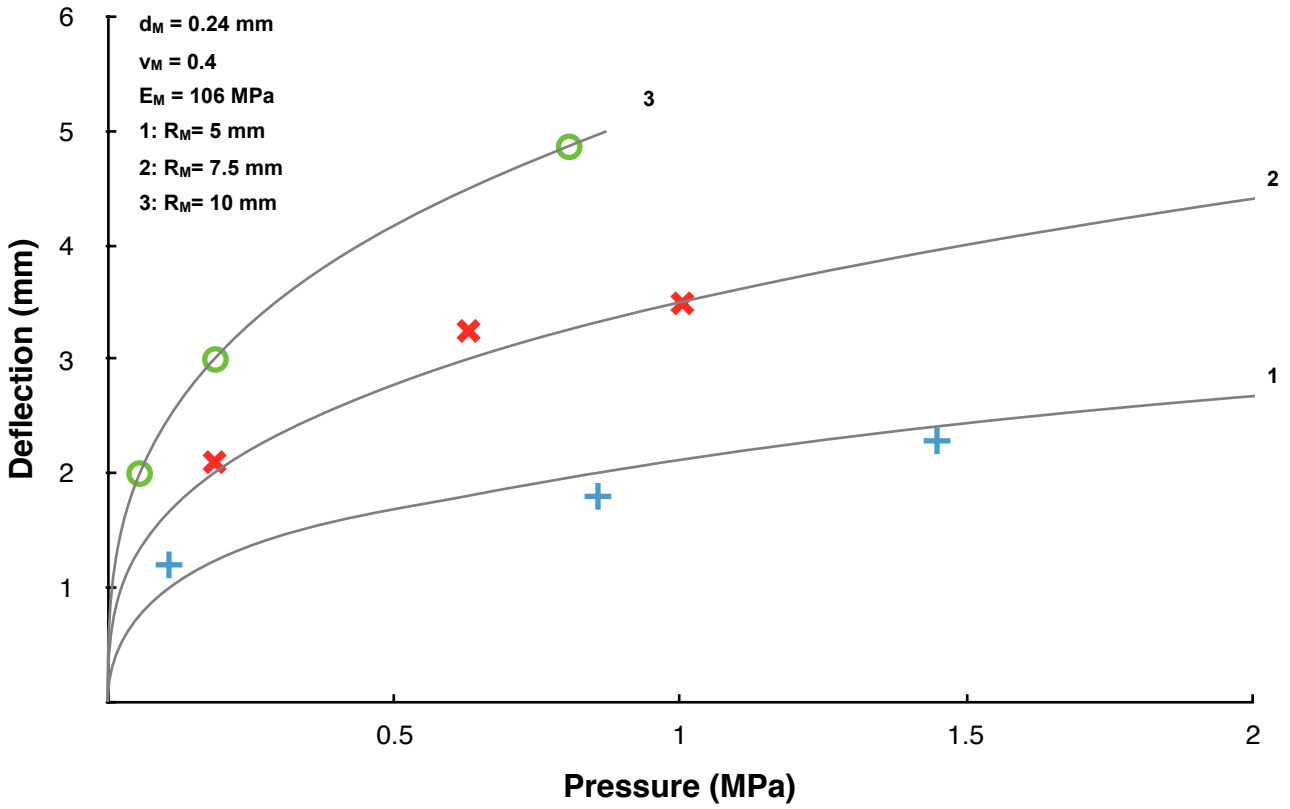

Figure 4.4 - Young's modulus as a function of the membrane sample radius at 50 % RH and 50 ℃.

From Figure 4.4 it is observed that the data points recorded for each radius correlates well to the model proposed by Schomburg (2011). Slight deviations from the theoretical values are observed for sample diameters of 5 mm and 7.5 mm. A root mean square deviation of 0.1 mm have been determined for the measured values compared to the model. This equates to a maximum deviation from the model of ± 7%, and good correlation with nearly no deviation from the model is observed for a sample radius of 10 mm. The model remains valid regardless of the radius of the membrane sample. Furthermore, it can be seen that the rupture pressure (last data points respectively) increases as the radius of the test sample decreases, whereas an increase in the deflection results from an increase of the test sample radius. A sample radius of 10 mm was used throughout further experimentation as it showed the best correlation.

From the results above it can be concluded that the experimental rig proposed for biaxial tensile testing is a valid alternative to conventional uniaxial tensile testing, and that the model of Schomburg can be used to related deflection with pressure.

4.2. Effect of environmental variation on the viscoelastic properties of Nafion®, reinforced and partially hydrolysed membranes.

The viscoelastic and mechanical properties of PEMs, as determined through biaxial tensile testing is discussed in Section 4.2. Section 4.2.1 will focus on the effect of temperature and RH on the viscoelastic properties of PEMs. Additional parameters influencing the viscoelastic and mechanical properties of the tested materials, such as sub-zero temperatures (Section 4.2.2), cation contamination (Section 4.2.3), membrane reinforcement (Section 4.2.4) and partially hydrolysed membranes (section 4.2.5), are also discussed.

4.2.1 Temperature and Relative humidity variation

The rupture pressure results of the biaxial tensile testing of NR115, NR117 and NR1110 conducted at 20 ℃, 50 ℃ and 80 ℃ with a RH level of 35 %, 50 %, 70 % and 90 % are presented in Figure 4.5 and Figure 4.6 as a function of RH and temperature respectively.

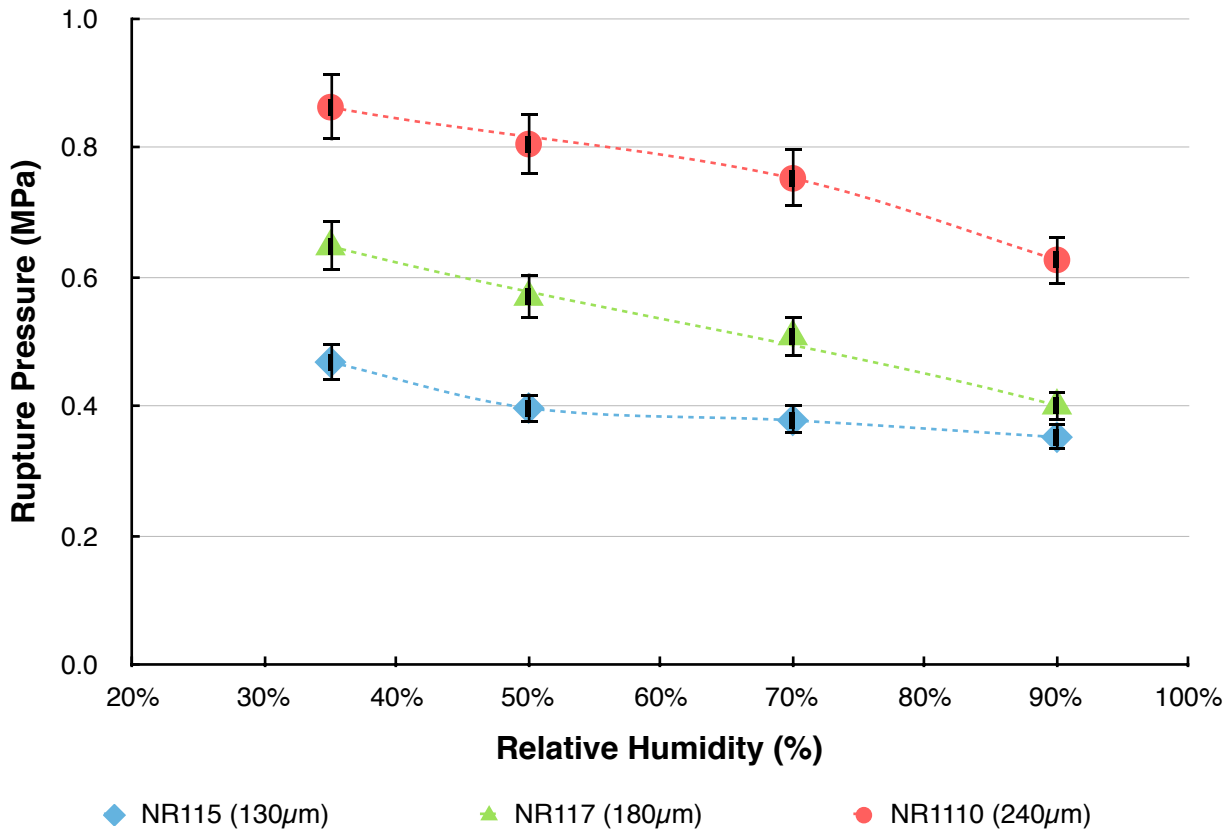

Figure 4.5 - Rupture pressure of non-reinforced Nafion® membranes as a function of RH at 50 °C.

In Figure 4.5 it is observed that the rupture pressure of the samples decreases as the thickness of the samples decreases and that the rupture pressure decreases with an increase of the RH at a constant temperature, which indicates that the water content of the membrane directly influences the rupture pressure. From Figure 4.6 it is observed that the rupture pressure decreases as the temperature increases at a constant RH level. When comparing Figure 4.5 and Figure 4.6 it is

seen that a change in the RH has a less significant effect on the rupture pressure than a change in temperature.

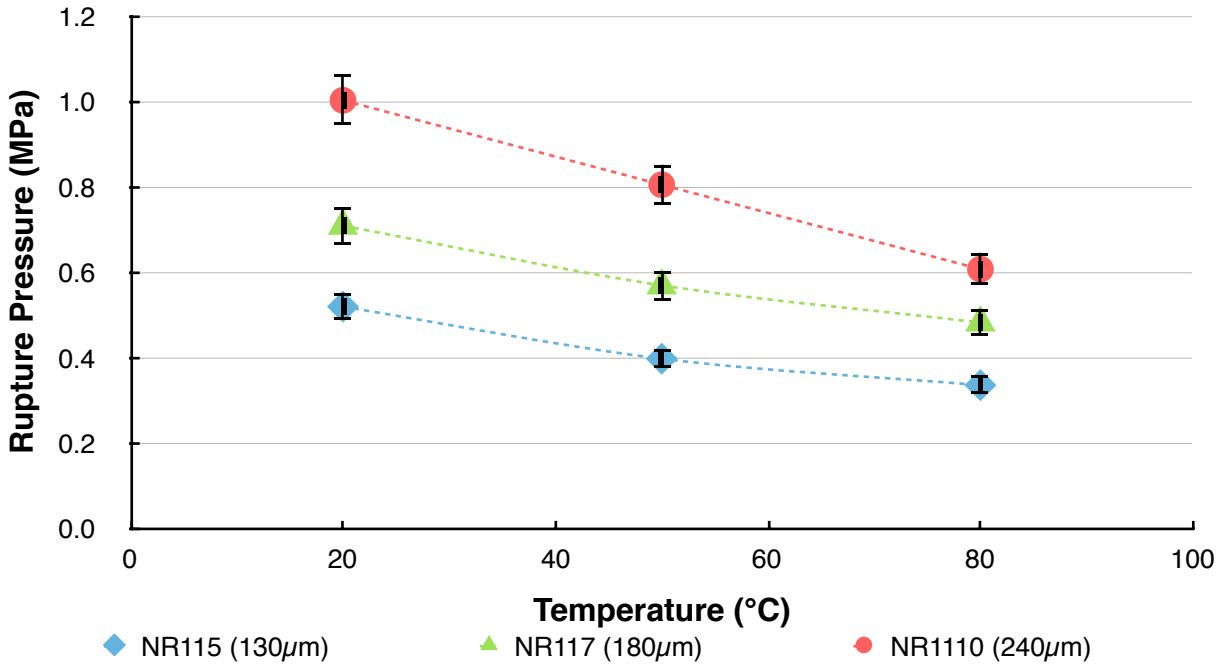

Figure 4.6 - Rupture pressure of non-reinforced Nafion® membranes as a function of temperature at 50 % RH.

The rupture pressure results from Figure 4.5 and Figure 4.6 along with the deflection measurements from the experimental procedures were used for the determination of the Young's modulus using Equation 2.4. These results for NR115, NR117 and NR1110 are presented in Table 4.2 for biaxial tensile testing at 20 ℃, 50 ℃ and 80 ℃ and RH levels of 35 %, 50 %, 70 % and 90 %.

Table 4.2 - Young's modulus of Nafion® membranes determined through biaxial tensile testing over a relative humidity range of 35 % to 90 % at 20 ℃, 50 ℃ and 80 ℃.

Membrane	Temperature (°C)	Relative humidity (%)			
		35%	50%	70%	90%
NR115	20	193	164	138	131
	50	135	106	89	79
	80	45	35	26	23
NR117	20	194	166	140	130
	50	131	105	90	82
	80	44	36	25	23
NR1110	20	197	168	142	133
	50	136	108	92	78
	80	45	32	27	22

From Table 4.2 it is observed that the Young's modulus remains constant for the three membrane species at a specific environmental condition, confirming the observation that the Young's modulus is not dependent on the thickness of the membrane. Therefore, it is possible to determine the average of Young's modulus of the three membrane species at each environmental condition and evaluate the results as representative of 1100 EW Nafion® membranes.

The results of the average of Young's modulus are presented in Figure 4.7.

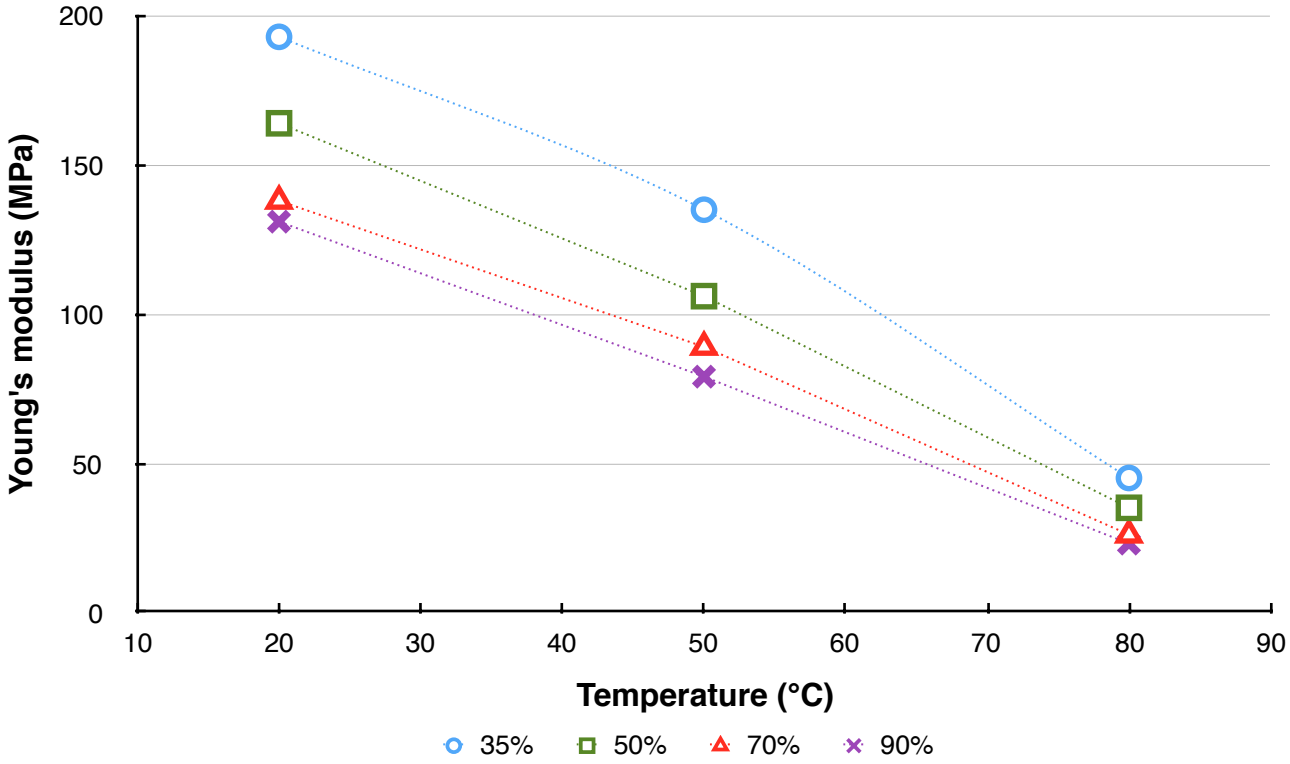

Figure 4.7 - Average Young's modulus of 1100 EW Nafion® membranes determined through biaxial tensile testing as a function of RH and temperature.

From Figure 4.7 it can be seen that the Young's modulus decreases with increases in both temperature and RH. This observation is expected as the Young's modulus is directly related to the rupture pressure (Figure 4.3 & Figure 4.4). The magnitude of the decrease due to temperature increase opposed to an increase in RH is also evident from Figure 4.7. The large decrease of the Young's modulus at increased temperatures can be attributed to the flexibility of the clusters (Satterfield, 2008). As the clusters become more flexible, the material becomes more susceptible to water uptake causing the stiffness of the membrane decreases, which results in a lower Young's modulus.

The decrease of the Young's modulus resulting from the RH increase can be attributed to the water within the hydrophilic domains reducing the strength of electrostatic bonds between sulfonate-groups which causes the polymer chains to plasticise. As a result, the stiffness of the membrane decreases, reducing the strength of the material.

The trend observed in Table 4.2 and Figure 4.7 is consistent with the sources presented in Table 2.4. The Young's modulus as a function of temperature and relative humidity in Figure 4.7 is compared to uniaxial tensile test results at similar conditions presented in in Table 2.1.

It is observed that the results obtained in Figure 4.7 compare well to the results obtained by Tang et al. (2006). The small difference between values can be contributed to the temperature and RH difference. It is also observed that the strain rate has nearly no effect on the Young's modulus, as an insignificant difference in values are observed for a strain rate of 0.2 mm/min by Tang et al. (2006) and 5 mm/min obtained in this study. Choi et al. (2006) and Kyrakides (2005) found values of 100 MPa higher for the Young's modulus at similar environmental conditions. The large difference in the values reported by the various authors is believed to be a result of the different pre-treatment methods. Data from the above mentioned authors are presented in Table 4.3 for ease of comparison.

Table 4.3 - Comparison of Young's modulus through biaxial testing to uniaxial tensile testing results from literature.

Researcher, Year	Material	Apparatus	Method	Water Content	Temp	Young's modulus [MPa]
Kirsten 2015	Nafion® 212, Nafion® 115, Nafion® 117, Nafion® 1110, no chemical pre-treatment	Gen-1 high-pressure gas membrane rupture system	Pre-conditioned for 30 min at selected conditions, Strain rate: 5mm/min	35% RH	20℃	196
				50% RH		167
				70% RH		141
				90% RH		133
				35% RH	50℃	135
				50% RH		106
				70% RH		89
				90% RH		79
				35% RH	80℃	45
				50% RH		35
				70% RH		26
				90% RH		23
Kyriakides 2005; Liu, Kyriakides *et al.,* 2006	Nafion® 117: pre treated boiling 0.5M H_2SO_4 2h & boiling DI water 2h, dried 70℃ vacuum, 40mm gauge length×12mm	Instron 4468 screw-driven universal testing machine, load cell: 1kN	Strain rate: 0.7/min	equilibrated at 23℃, 40%RH 72h, water concentration: 5.3±1.5%	23℃	270 ± 4
			Strain rate: 0.3/min			253 ± 7
			Strain rate: 0.12/min			256 ± 18
			Strain rate: 0.07/min			263 ± 10
			Strain rate: 0.025/ min			250 ± 5
				30% RH	25℃	~230
				50% RH		~180
				70% RH		~150

Tang *et al.,* 2006	Nafion® 112: pre treated boiling 3%H_2O_2, 0.5M H_2SO_4 and DI 1hr, 50mm gauge length×10mm	MTS Alliance RT/5 material testing system	Strain rate: 0.2/min	90% RH		~110
				30% RH	45℃	~170
				50% RH		~147
				70% RH		~122
				90% RH		~80
				30% RH	85℃	~83
				50% RH		~75
				70% RH		~60
				90% RH		~45
Choi *ei al.,* 2006	Nafion® 112	Thermal analysis 2980 DMA instrument	OEH Technique	10% RH	40℃	~280
				40% RH		~240
				60% RH		~210
				90% RH		~190
				10% RH	60℃	~245
				40% RH		~210
				60% RH		~190
				90% RH		~160
				10% RH	80℃	~120
				40% RH		~100
				60% RH		~90
				90% RH		~80

4.2.2. Sub-Zero Temperatures

NR1110 samples were used, as representative of the 1100 EW Nafion® materials, to investigate the viscoelastic properties of the material at sub-zero temperatures. The rupture pressure of the specimens were recorded at sub-zero temperatures and compared with results recorded at more conventional operating temperatures at 50% RH. The results are presented in Figure 4.8.

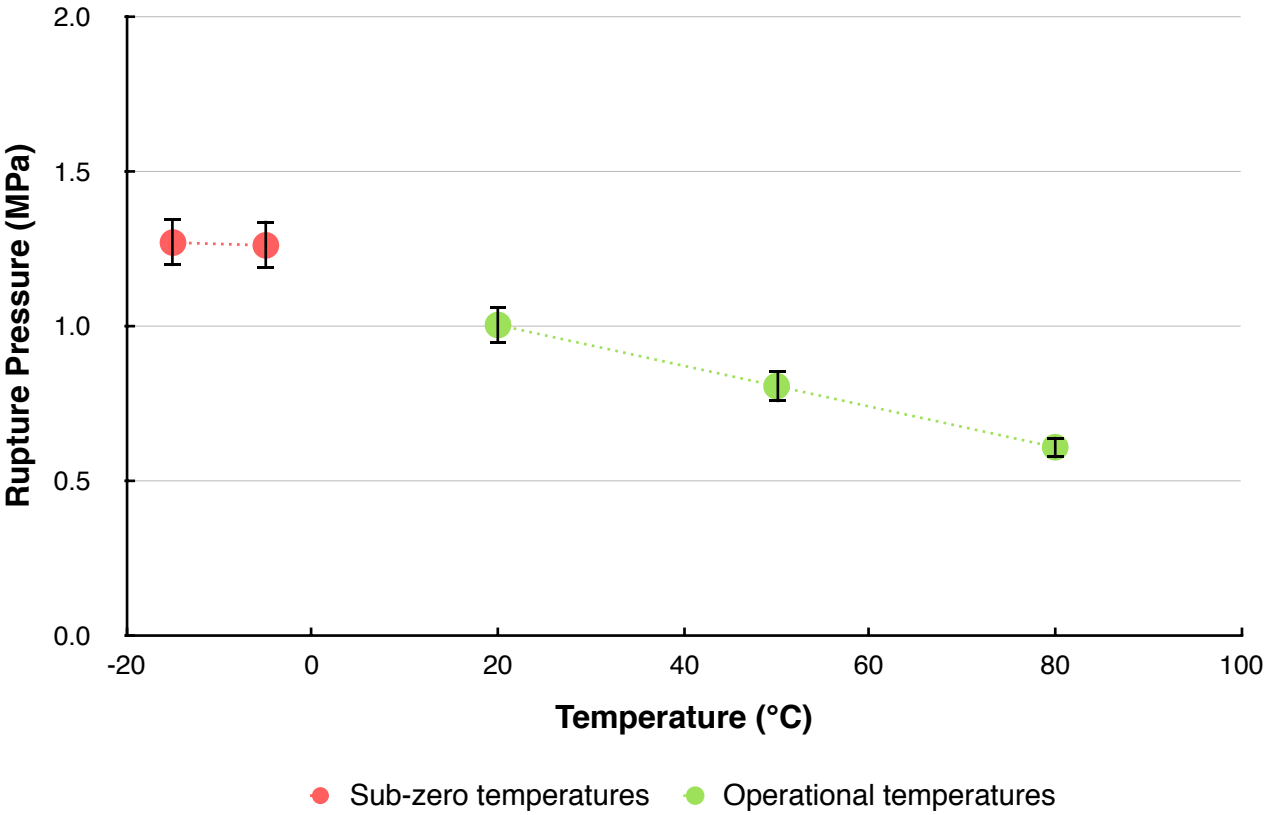

Figure 4.8 - Rupture pressure of NR1110 at sub-zero temperatures and ~53 ± 2 %RH compared to operational temperatures of electrochemical hydrogen energy systems at 50 % RH.

In Figure 4.8 it is observed that there is no significant difference between the rupture pressure of the membrane samples at -15 ℃ compared to -5 ℃, and that at the rupture pressure of both sub-zero temperatures are higher than the values obtained at temperatures above 0 ℃. It seems that the decrease in the rupture pressure with an increase in temperature observed for the more conventional temperatures disappears for temperatures < 0 ℃.

Due to the insignificant increase in the rupture pressure observed between -5 ℃ and -15 ℃ in Figure 4.8 the presence of non-freezable water, that shows minimal- to no thermal transition inside the membrane matrix at sub-zero temperatures, can not be confirmed. Further testing with more sensitive apparatus will be required.

4.2.3. Cation Impurities

NR1110 samples were used, as representative of the Nafion® materials, to investigate the effect of foreign metal cations on the rupture pressure and Young's modulus of the material. The Young's modulus results of samples subjected to cation exchange at 50 ℃ and 50 % RH are presented in Figure 4.9.

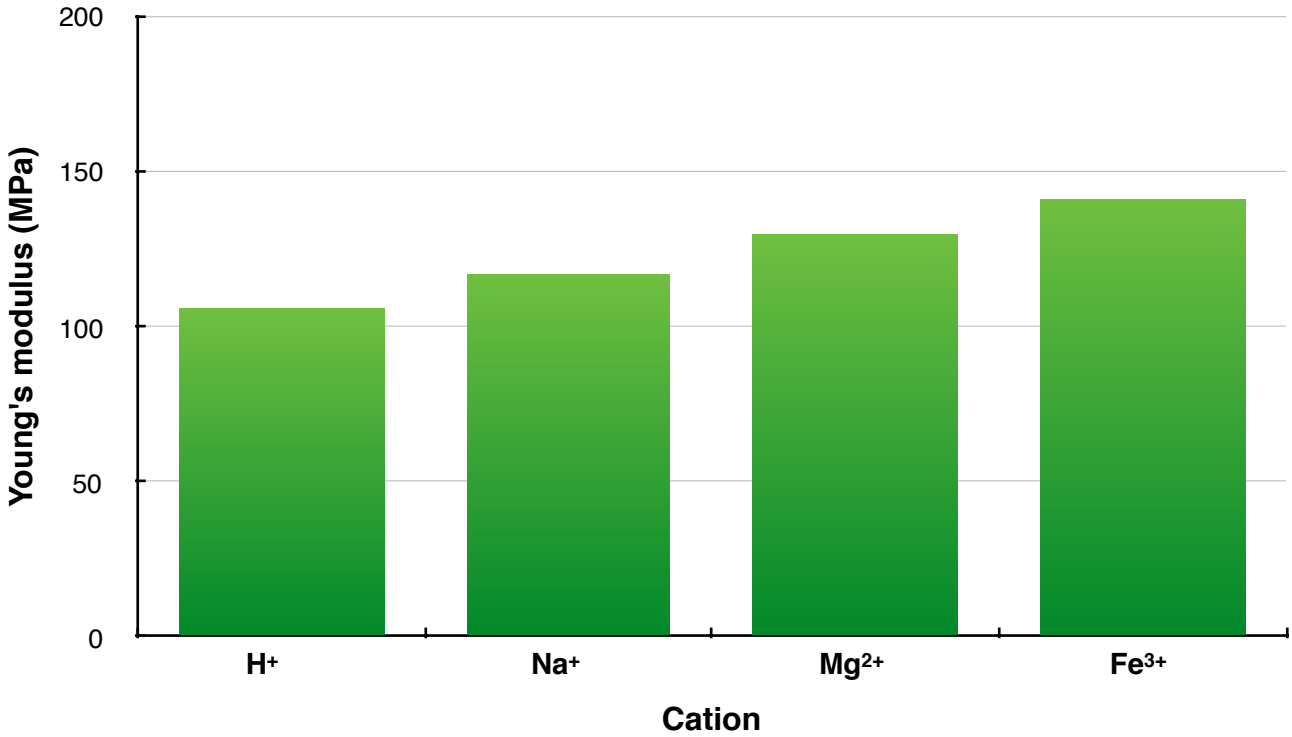

Figure 4.9 - Young's modulus of non-reinforced Nafion® 1110 (240µm) membranes subjected to ion exchange at 50 °C and 50 % RH.

From Figure 4.9 it is observed that the Young's modulus of the samples increase in the order H^+, Na^+, Mg^{2+}, Fe^{3+}. The increase in the Young's modulus can be attributed to several factors, which are based on the premise that the mechanical and viscoelastic properties of Nafion® are mainly dependent on the water content in the membrane. Properties of the cations used for cation exchange are provided in Table 4.4.

Table 4.4 - Properties of ions used for the contamination of Nafion® 1110 membranes.

	H^+	Na^+	Mg^{2+}	Fe^{3+}
Young's modulus (MPa)	106	117	130	141
Valence	1	1	2	3
Ionic radius (pm) (Kotz *et al., 2009)*	53	102	72	60
Charge Density	0.019	0.010	0.028	0.038

The reference membrane for the contamination tests contains only the H^+ cation, and all the sulfonic acid groups are occupied by the H^+ ions within the matrix of the membrane. This physical structure allows for maximum uptake of water due to the formation of hydronium ions, weakening the membrane.

As a result of cation exchange, the sulfonic acid groups are occupied by cations other than H^+, which affects the water uptake of the material. The presence of the cation causes the mobility of the sulfonic acid groups to decrease, lowering the flexibility of the side chains around the cluster which results in the structural stiffness and consequently the Young's modulus of the membrane to increase (Kundu *et al.,* 2005). When multivalent cations such as magnesium and iron are used in the contamination process, it is believed that two or even three acid sites are attached to the metal ion (Jia *et al.,* 2012). This effect reduces the overall water uptake of the membrane, and hence increases the strength. There is thus a correlation between the Young's modulus, ion valence and charge density . Similar results have been reported by Collier *et al.* (2006), Jai *et al.* (2012) and Kundu *et al*. (2005).

4.2.4. Reinforced membranes

Reinforced membranes supplied by OEM1 (50 µm and 60 µm) and Fumatech (90 µm, 130 µm, 240 µm and 360 µm) were tested to investigate the effect of reinforcement on the mechanical strength of the Nafion-based membrane materials. The rupture pressures were recorded and are compared to that of non-reinforced Nafion® membranes of similar thickness at 50 ℃ and 90 % RH. The results are presented in Figure 4.10.

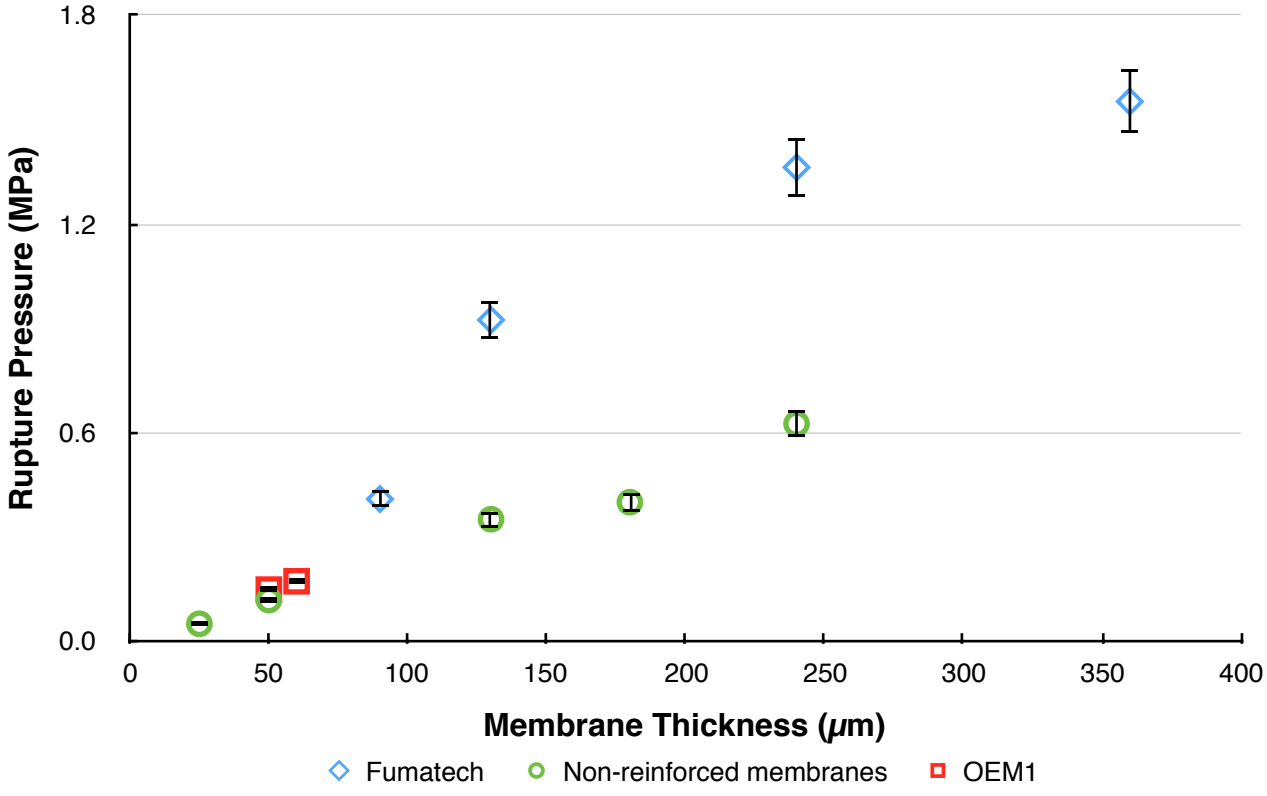

Figure 4.10 - Rupture pressure of reinforced membranes compared to non-reinforced Nafion® membranes of similar thickness at 50°C and 90% RH.

From Figure 4.10 it is observed that the rupture pressure of the Fumatech samples are almost two times larger than that of the non-reinforced Nafion® samples. The samples supplied by OEM1 however, do not show a similar significant increase of the rupture pressure.

The Fumatech reinforced membranes are cast on a homogeneous ePTFE film layer with more closely spaced nodes, interconnected with a greater number of fibrils which provides the samples with increased mechanical strength. OEM1 did not disclose the method used for the reinforcement of their material. However from the results it can be concluded that the reinforcement introduced by OEM1 is less effective than that of Fumatech.

A reinforced membrane sample from Fumatech after rupture at 50 ℃ and 90 % RH is shown in Figure 4.11. From this figure the support inside the specimen, responsible for the increase of strength, is clearly visible.

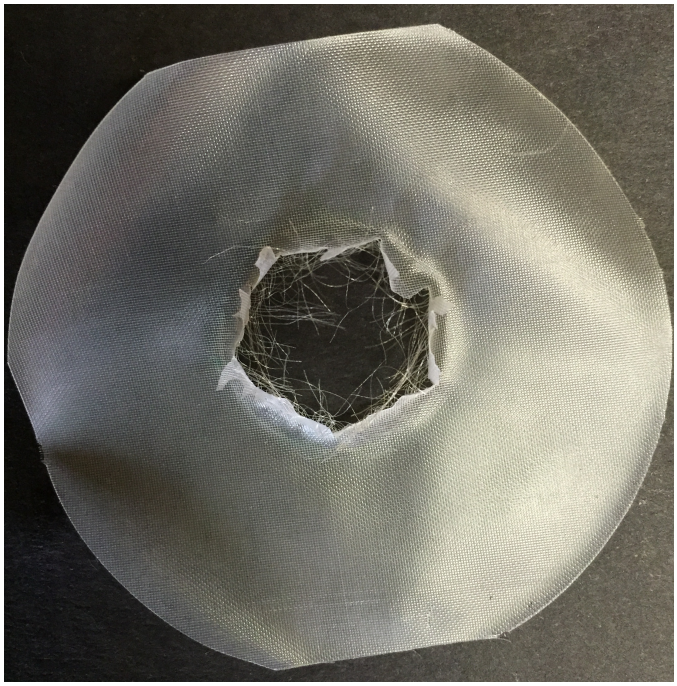

Figure 4.11 - Reinforced membrane (Fumatech) after rupture conducted through biaxial tensile testing at 50 ℃ and 50 % RH.

4.2.5. Partially Hydrolysed Membranes

Non-hydrolysed membranes (110 μm) supplied by PlastPolymer were partially hydrolysed over different periods of time to alter the chemical structure of the samples. The hydrolysis procedure is explained in section 3.3.4, and the results of the equivalent weight (EW) as a function of the hydrolysis time are presented in Figure 4.12.

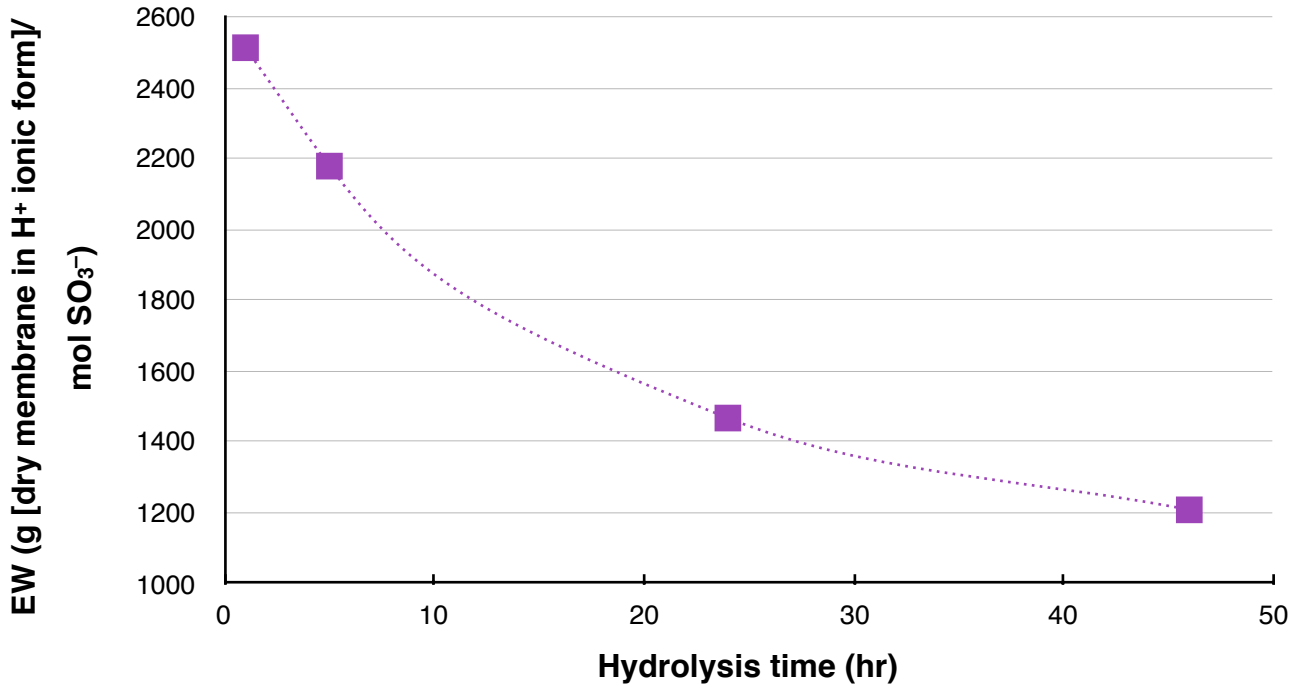

Figure 4.12 - Influence of hydrolysis time on the equivalent weight (EW) of a non-hydrolysed membrane (110µm).

In Figure 4.12 it can be seen that EW of the samples decreases as the hydrolysis time is extended. The chemical structure of non-hydrolysed membranes becomes more like that of PFSA membranes when hydrolysed; SO_2—F end groups are replaced by SO_3—H. The equivalent weight (EW) stabilised to 1200 g/mol.SO_3^-, after about 46 hours, which is the EW of a typical Nafion® membrane. As the period of hydrolysis is extended the runs of tetrafluoroethylene become of sufficient length to organise into crystalline domains with dimensions identical to that of pure PTFE, resulting in a more stable chemical structure.

The rupture pressure as a function of the EW of the partially hydrolysed membranes at 50 ℃ and 50% RH is presented Figure 4.13.

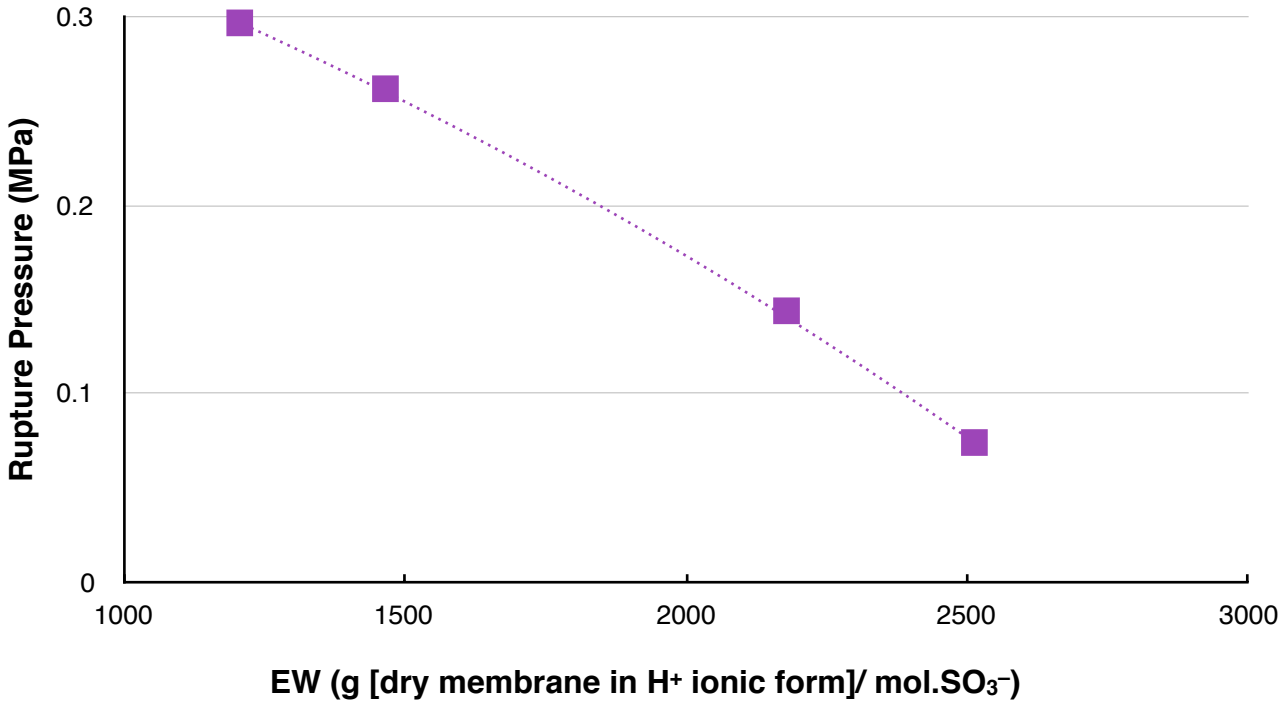

Figure 4.13 - Rupture pressure as a function of the equivalent weight of partially hydrolysed membranes (110µm) at 50 °C and 50 % RH.

From Figure 4.13 it can be seen than an increase in rupture pressure is observed with a decrease in the EW of the material. Therefore, it can be concluded that the chemical transformation resulting from the hydrolysis, influences the strength of the membrane. This observation can be explained by the electronegativity of the end groups and water. The SO_2—F end groups are partially more negative than the SO_3—H end groups due to the presence of fluorine ion, opposed to the additional oxygen ion (Kotz *et al.,* 2009). As a result the SO_2—F has a greater affinity to interact with the partially positive end of the water molecules than SO_3—H. Therefore, the unhydrolyzed perfluorinated membrane has a higher water content than the hydrolysed membrane, resulting in reduced strength.

4.2.6. Summary

In Section 4.1 it was shown that the biaxial tensile testing method is comparable to conventional uniaxial tensile testing, and that the data correlates well to the theoretical model proposed by Schomburg (2011). Section 4.2. showed that the viscoelastic properties are mainly influenced by the water content of the material. RH, temperature and cation contamination were shown to negatively influence the Young's modulus of the materials whilst mechanical reinforcement improved the strength of the PEMs. The membranes were still strong at sub-zero temperatures due to minimal thermal transition of water at such low temperatures and that the Young's modulus of PEM materials are not dependent on the thickness.

Chapter 5 - Conclusions and recommendations

An introduction to different PEM materials and how their mechanical and viscoelastic properties can be determined were presented in Chapter 2. Details of the experimental setup, materials and experimental procedures were discussed in Chapter 3. The results recorded during experimental procedures were provided and discussed in Chapter 4. The main Conclusions drawn from the experimental results in Chapter 4 will be summarised in Section 5.1. Recommendations with regards to future work to be done in this field of study are discussed in Section 5.2.

5.1. Conclusions

A biaxial tensile testing method suited for the characterisation of PEMs was developed and constructed through a high-pressure gas membrane rupture test. It was shown that by the use of the model proposed by Schomburg (2011) the viscoelastic properties of PEMs could be determined accurately. The biaxial testing method was used to determine the Young's modulus, with the results comparable to that obtained through uniaxial tensile testing.

It can be concluded that the rupture pressure and Young's modulus are directly related to each other. It was shown that the Young's modulus of Nafion® membranes remains constant at a specific environmental condition regardless of the thickness of the membrane. These tests also showed that the Young's modulus, and therefore the rupture pressure decreases with an increase relative humidity and temperature. It was further shown that the Young's modulus of 1100 EW Nafion® membranes range between 0 - 200 MPa at temperatures of 20 ℃ to 80 ℃ and RH levels of 35% to 90 %. These values were also shown to correlate well to literature. It was shown that the mechanical properties of the non-reinforced Nafion membranes did not change significantly at temperatures < 0 ℃, and that the Young's modulus was larger at temperatures < 0 ℃ than at temperatures > 0 ℃. Although, hydrogen technology operation such as electrochemical hydrogen compression are not conducted at sub-zero temperatures, it is a requirement of the technologies to be able to initiate start up at such conditions. These results indicate that it would be possible as there is still water content within the membrane at these conditions.

Further it can be concluded that as a result of ion exchange, the Young's modulus and mechanical strength of the non-reinforced Nafion membranes are increased. Although there is an increase in strength, contamination of the Nafion® membrane is an undesired variable, as it prevents conductive pathways from being formed, reducing the efficiency of proton conductivity across the matrix during operation of electrochemical hydrogen energy systems.

Reinforced membranes supplied by Fumatech were shown to be superior to non-reinforced membrane samples, as they exhibited a 100 % rupture pressure increase compared to non-reinforced membranes of similar thickness. Additionally it was shown that some methods of reinforcement are less effective than others, as the reinforced membranes supplied by OEM1 did not show the same improvement in the rupture pressure as those supplied by Fumatech.

Fully hydrolysed membranes were shown to exhibit much greater mechanical strength, due to a more stable matrix, than non-hydrolysed perfluorinated membranes. It was further observed that the EW of non-hydrolysed membranes decrease when the membranes become partially hydrolysed as a result of hydrolysis. Therefore, the fully hydrolysed membrane, i.e. Nafion® is the preferred membrane for membrane-based electrochemical hydrogen energy systems.

In conclusion this research has provided a data set on the Young's modulus of non-reinforced Nafion membranes over an extensive range of environmental conditions, to provide a better understanding of the behaviour of the membrane material as a function of temperature and relative humidity. Further, parameters such as sub-zero temperatures and cation contamination were explored, to show that the viscoelastic and mechanical properties of proton exchange membranes are influenced by more operational variables of electrochemical hydrogen energy systems than simply temperature and RH. It was further shown that reinforcement of PFSA materials can significantly increase the mechanical strength of the material, and that the final hydrolysis step in the fabrication of PFSA materials is a vital in the stabilisation of the chemical of PFSA materials. Although the surface of the influence of these parameters were only scratched it indicated that much more research is required to fully understand PFSA materials. By further exploring these parameters, the behaviour of PFSA materials will be better understood, providing a basis for achieving the durability requirements for membranes used within electrochemical hydrogen energy systems.

5.2. Recommendations

With regards to the experimental setup the following recommendations are made:

- A mass flow meter can be inserted to more accurately determine the rate of pressurisation. Although it was not of great importance in the current study, as the rate of pressurisation was shown to not influence the rupture pressure of the membrane, it would be an extra element of control within the system. This would also improve the automation, allowing for more accurate testing on thinner membrane samples, which might require low flow rates from the baseline gas.
- Future experiments, done in a similar fashion, should incorporate a device that digitally measures the defection. By introducing a device that can digitally measure the deflection, the system would be completely automated, as a result this could eliminate possible human error which would improve the accuracy of the procedure.

With regards to future work on membrane strength characterisation for hydrogen technologies, specifically electrochemical hydrogen compression, the following recommendations are made:

- Future experimental work must be done with membrane support. Although the experiment as it currently stand, provides valuable information with regards to the characteristics of the membrane itself, it lacks the ability to be directly related to a membrane functioning within the hydrogen technology device. This is due to the fact that the PEM, for example inside a electrochemical hydrogen compressor, is entirely constrained, and is not able to deflect in any manner. It is recommended that support similar to that found within the hydrogen technologies is incorporated with the high pressure cell.
- Future experimental work must be done on membranes with a catalyst layer. Although, this would be very expensive, it would provide valuable information with regards to the effect the catalyst layer has on the mechanical properties of the membrane.

- A greater variety of cation contaminants can be tested to investigate whether there are other correlations between the Young's modulus and a specific cation.
- Further characterisation results on the effect of strain on other membrane properties relating to the implications faced within operating fuel cell assemblies can be investigated.

Bibliography

Abuin, G.C., Fuertes, M.C. & Corti, H.R. 2013. Substrate effect on the swelling and water sorption of Nafion® nano-membranes. *Journal of Membrane Science,* 428:507-515.

Afrox. Material safety data sheets. http://www.afrox.com/internet.global.corp.zaf/en/images/Nitrogen266_92463. Date of access: 08 Aug. 2015.

Anderson, E., Ayers, K. & Capuano, C. 2013. R&D focus areas based on 60000hr life PEM electrolysis stack experience. Presented at First International Workshop on Durability and Degradationn Issues in PEM Electrolysis Cells and its Components, Freiburg, Germany.

Andrews, N., Knights, S., Murray, K., Mcdermid, S., MacKinnon, S. & Ye, Y. 2005. (Patent: US 20050136308 A1).

Barbir, F. 2013. PEM fuel cells: Theory and practice. Elsevier. http://www.sciencedirect.com/science/article/pii/B9780123877109050025. Date of access: 01 Apr. 2015.

Barbir, F. & Gorgun, H. 2007. Electrochemical hydrogen pump for recirculation of hydrogen in a fuel cell stack. *Journal of Applied Electrochemistry,* 37:359-365.

Bauer, F.; Denneler, S.; Willert-Porada, M. 2005. Influence of temperature and humidity on the mechanical properties of Nafion® 117 polymer electrolyte membrane. *Journal of Polymer Science Part B-Polymer Physics,* 43(7), 786-795.

Beams, J.W. 1959. Mechanical properties of thin films of gold and silver. *The structure and properties of thin films*, 183–192.

Bessarabov, D.G., Micheals, W. & Sanderson, R.D. 2000. Preparation and characterisation of chemically-modified perfluorinated cation-exchange platinum-containing membranes. *Journal of Membrane Science,* 179:221-229.

Bessarabov, D.G. & Kozak, P. 2007. Measurement of gas permeability in SPE membranes for use in fuel cells. *Membrane technology*, December: 6-9.

Bose, S., Luila, T., Nguyen, T.X.H., Kim, N.H., Lau, K. & Lee, J.H. 2011. Polymer membranes for high temperature proton exchange membrane fuel cell: Recent advances and challenges. *Progress in Polymer Science,* 36:813-843.

Bromley, E.I., Randall, J.N., Flanders, D.C. & Mountain, R.W. 1983. A technique for the determination of stress in thin films. *Journal of Vacuum Science and Technology,* 4(1): 1364-11366.

Campos, H., Santos, A., Martins, B., Ito, K., Mori, N. & Barlat, F. 2014. Hydraulic bulge test for stress-strain curve determination and damage calibrationn for ito-goya model. 11th World congeess on computational mechanics.

Carmo, M., Fritx, D.L., Mergel, J. & Stolten, D. 2013. A comprehensive review on PEM water electrolysis. *International Journal of Hydrogen Energy,* 38:4901-4934.

Casati, C., Longhi, P., Zanderighi, L. & Bianchi, F. 2008. Some fundamental aspects in electrochemical hydrogen purification/compression. *Journal of Power Sources,* 180:103-113.

Cheng, X., Shi, Z., Glass, N., Zhang, L., Zhang, J., Song, D., Liu, Z., Wang, H. & Shen, J. 2007. A review of PEM hydrogen fuel cell contamination: Impacts, mechanisms and mitigation. *Journal of Power Sources,* 165:739-756.

Choi, P., Jalani, N.H., Thampan, T.M. & Datta, R. 2006. Consideration of thermodynamic, transport and mechanical properties in the design of polymer electrolyte membranes for higher temperature fuel cell operation. *Journal of Polymer Science: Part B: Polymer Physics*, 44:2183-2200.

Clough, N.E. Inovations in ePTFE fiber technology: New capabilities, new applications, new opportunities. W.L. Gore & Assoiciates, Inc. http://www.gore.com/mungoblobs/168/901/ ePTFE_innovations_paper.pdf. Date of access: 24August 2015.

Collier, A., Wang, H., Yuan, X., Zhang, J. & Wilkinson, D.P. 2006. Degradation of polymer electrolyte membranes. *International Journal of Hydrogen Energy,* 31:1838-1854.

Devore, J. & Farnum, N. 2005. Applied statistics for engineers and scientists. 2nd ed. Belmont,CA: Brooks/Cole.

Edwards, R.L., Coles, G. & Sharpe, W.N. 2004. Comparison of tensile and bulge tests for thin-film siliconn nitrade. *Experimental Mechanics,* 44:49-54.

Fujimoto, C.H., Hickner, M.A., Cornelius, C.J. & Loy, D.A. 2005. Ionomeric poly (phenylene) prepared by diels-alder polymerization:Synthesis and physical properties of a novel polyelectrolyte. *Macromolecules* 38(12):5010-5016.

Gore, W.L. 1969. Sealing materials. (Patent: US 3664915).

Gore, R.W. 1976. Very highly stretched polytetrafluoroethylene and process therefor. (Patent: US 3962153).

Gore, R.W. 1976. Process for producing porous products. (Patent: US 3953566).

Gore, R.W. 1978. Process for producing filled porous PTFE products. (Patent: US 4096227).

Gore, R.W. 1980. Porous products and the process therefor. (Patent: US 4187390).

Grigoriev, S.A., Shtatniy, I.G., Millet, P., Porembsky, V.I. & Fateev, V.N. 2011. Description and characterisation of an electrochemical hydrogen compressor/concentrator based on solid polymer electrolyte technology. *International Journal of Hydrogen Energy,* 36(6):4148-4155.

Grohs, J.R., Li, Y., Dillard, D.A., Case, S.W., Ellis, M.W., Lai, Y. & Gittleman, C.S. 2010. Evaluating the time and temperature dependant biaxial strength of Gore-Select® series 57 proton exchange membrane using a pressure loaded blister test. *Journal of Power Sources,* 195:527-531.

Grot, W. 2008. Fluorinated Ionomers. 1st ed. Norwich, NY: William Andrew Publishing.

Guerra, M.A. & Yandrasits, M.A. 2008. Reinforced polymer electrolyte membrane. (Patent: US 7411022 B2).

Guo, S., Wan, K. & Dillard, D.A. 2005. A bending-to-stretching analysis of the blister test in the presence of tensile residual stress. *International Journal of Solids and Structures,* 42:2771-2784.

Guvelioglu, G.H. & Stenger, H.G. 2007. Flow rate and humidification effects on a PEM fuel cell performance and operation. *Journal of Power Sources,* 163(2):882-891.

Hamdan, M. 2014. High pressure PEM electrolysis. Presented at Electrolytic Hydrogen Production Workshop NREL, Golden, Colorado.

Hockday, R.G. 1995. Surface replica fuel cell. (Patent: US 5631099).

Inaba, M., Kinumoto, T., Kiriake, M., Umebayashi, R., Tasaka, A. & Ogumi, Z. 2006. Gas crossover and membrane degradation in polymer electrolyte fuel cells. *Electrochemica Acta,* 51:5746-5753.

Ito, H., Maeda, T., Nakano, A. & Takenaka, H. 2011. Properties of Nafion® membranes under PEM water electrolysis conditions. *International Journal of Hydrogen Energy,* 36:10527-10540.

Jia, R., Han, B., Levi, K., Hasegawa, T., Ye, J. & Dauskardt, R.H. 2011. Effect of cation contamination and hydrated pressure loading on the mechanical properties of proton exchange membranes. *Journal of Power Sources*, 196:3803-3809.

Jia, R., Dong, S., Hasegawa, T., Ye, J. & Dauskardt, R.H. 2012. Contamination and moisture absorption effects on the mechanical properties of catalyst coated membranes in PEM fuel cells. *International Journal of Hydrogen Energy,* 37:6790-6797.

Jian, Q., Ma, G. & Qiu, X. 2014. Influence of gas relative humidity on the temperature of membrane in PEMFC with integrated flow field. *Renewable Energy,* 62:129-136.

Jiao, K. & Li, X. 2001. Water transport in polymer electrolyte membrane fuel cells. *Progress in Energy and Combustion Science,* 37:3120-3124.

Kawano, Y., Wang, Y.Q., Palmer, R.A. & Aubuchon, S.R. 2002. Stress-strain curves of Nafion® membranes in acid and salt forms. *Polimeros: Ciencia e Technologia*, 12(2):96-101.

Kim, Y.S., Dong, L., Hickner, M.A., Glass, T.E., Webb, V. & McGrath, J.E. 2003. State of water in disulfonated poly (arylene ether sulfone) copolymers and a perfluorosulfonic acid copolymer (Nafion®) and its effect on physical and electrochemical properties. *Macromolecules*, 36(17): 6281-6285.

Kotz, J.C., Treichel, P.M. &Townsend, J.R. 2009. Chemistry & chemical reactivity. 7th ed. Belmont,CA: Thomson.

Kundu, S., Simon, L.C., Fowler, M. & Grot, S. 2005. Mechanical properties of Nafion®(TM) electrolyte membranes under hydrated conditions. *Polymer,* 46(25):11707-11715.

Kyriakides, S.A. 2005. Mechanical behavior of Nafion® and BPSH membranes. *Journal of Undergraduate Materials Research*, 1:11-14.

Li, H., Tsay, K., Wang, H., Shen, J., Wu, S., Zhang, J., Jia, N., Wessel, S., Abouatallah, R., Joos, N. & Schrooten, J. 2010. Durability of PEM fuel cell cathode in the presence of Fe^{3+} and Al^{3+}. *Journal of Power Sources,* 195:8089-8093.

Li, H. Zhang, S., Qian, W., Yu, Y., Yuan, X., Wang, H., Jaing, M., Wessel, S. & Cheng. 2012. Impacts of operating conditions on the effect of chloride contamination on PEM fuel cell performance and durability. *Journal of Power Sources,* 218:375-382.

Li, Y. 2008. Experimental studies on the mechanical durability of proton exchange membranes. Virginia: VA. (Thesis - PhD).

Li, Y., Quincy, J.K., Case, S.W., Ellis, M.W., Dillars, D.A., Lai, Y., Budinski, M.K. & Gittleman, C.S. 2008. Characterising the fracture resistance of proton exchange membranes. *Journal of Power Sources,* 185:374-380.

Li, Y., Dillard, D.A., Case, S.W., Ellis, M.W., Lai, Y., Gittleman, C.S. & Miller, D.P. 2009. Fatigue and creep to leak tests of proton exchange membranes using pressure loaded blisters. *Journal of Power Sources,* 194:873-879.

Li, Y., Grohs, J.R. & Case, S.W. 2009. On the use of pressure-loaded blister tests to characterise the strength and durability of proton exchange membranes. *Journal of Fuel Cell Science and Technology,* 6:0310141-0310148.

Liu, D., Kyriakides, S., Case, S.W., Lesko, J.J., Li, Y.X. & McGrath, J.E. 2006. Tensile behavior of Nafion® and sulfonated poly (arylene ether sulfone) copolymer membranes and its morphological correlations. *Journal of Polymer Science Part B-Polymer Physics,* 44(10):1453-1465.

Liu, W., Ruth, K. & Rusch, G. 2001. Membrane durability in PEM fuel cells. *Journal of New Materials for Electrochemical Systems,* 4:227-231.

Maldonado, L., Perrim, J., Dillet, J. & Lottin. 2012. Characterisation of polymer electrolyte Nafion® membranes: Influence of temperature, heat treatment and drying protocol on sorption and transport properties. *Journal of Membrane Science,* 389:43-56.

Merle, B. 2013. Mechanical properties of thin films studied by bulge testing. Erlangen: FAU. (Thesis - PhD).

Moukheiber, E., De Moor, G., Flandin, L. & Bas, C. 2012. Investigation of ionomer structure through its dependence on ion exchange capacity (IEC). *Journal of Membrane Science,* 389:294-304.

Moukheiber, E., Bas, C. & Flandin, L. 2014. Understanding the formation of pinholes in PSFA membranes with the essential work of fracture (EWF). *International Journal of Hydrogen Energy,* 39:2717-2723.

Naudy, S., Collette, F., Thominette, F., Gebel, G. & Espuche, E. 2014. Influence of hygrothermal aging on the gas and water transport properties of Nafion® membranes. *Journal of Membrane Science,* 451:293-304.

Oda, Y., Morimoto, T. & Suzuki, K. 1987. Ion exchange membrane cell and electrolytic process using thereof. (Patent: US 4666574 A).

Onda, K., Ichihara, K., Nagahama, M., Minamoto, Y. & Araki, T. 2007. Separation and compression characteristics of hydrogen by use of proton exchange membrane. *Journal of Power Sources,* 164:1-8.

Patankar, K.A. 2009. Linear and non-linear viscoelastic characterisation of proton exchange membranes and stress modeling for fuel cell applications. Virginia: VA. (Thesis - PhD).

Patil, Y.P., Jarrett, W.L. & Mauritz, K.A. 2010. Deterioration of mechanical properties: A cause for fuel cell membrane failure. *Journal of Membrane Science,* 356:7-13.

Petrina, S.A. 2013. Water sorption, viscoelastic and optical properties of thin Nafion® films. Pennsylvania: PA. (Thesis - PhD).

Radhakrishnan, V. & Haridoss, P. 2010. Effect of cyclic compression on structure and properties of a gas diffusion layer used in PEM fuel cells. *International Journal of Hydrogen Energy,* 35:11107-11118.

Rikukawa, M. & Sanui, K. 2000. Proton-conducting polymer electrolyte membranes based on hydrocarbon polymers. *Progress in Polymer Science,* 25:1463-1502.

Rohland, B., Eberle, K., Ströbel, R., Scholta, J. & Garche, J. 1998. Electrochemical hydrogen compressor. *Electrochemica Acta,* 43(24):3841-3846.

Roy, S., Zorman, C. & Mehregany, M. 2006. The mechanical properties of polycrystalline 3 C-SiC flims grown on polysilicon substrates by atmospheric pressure chemical-vapour deposition. *Journal of Applied Physics,* 99:0441081-04410813.

Satterfield, M.B. & Benziger, J.B. 2008. Viscoelastic properties of Nafion® at elevated temperature and humidity. *Journal of Polymer Science: Part B: Polymer Physics,* 47:11-24.

Schalenbach, M., Carmo, M., Fritz, D.L., Mergel, J. & Stolten, D. 2013. Pressurised PE< water electrolysis: Efficiency and gas crossover. *International Journal of Hydrogen Energy,* 38:14921-14933.

Schomburg, W.K. 2011. Introduction to microsystem design. Berlin Heidelberg: Springer-Verlag. http://www.springer.com/gp/book/9783642194887. Date of access: 01 Apr. 2015.

Shi, S., Chen, G., Wang, Z. & Chen, X. 2013. Mechanical properties of Nafion® 212 proton exchange membrane subjected to hygrothermal aging. *Journal of Power Sources,* 238:318-323.

Sigma-Aldrich. Material safety data sheets. http://www.sigmaaldrich.com/MSDS. Date of access: 08 Aug. 2015.

Skoog, D.A., West, D.M., Hollar, F.J. & Crouch, S.R. 2004. Fundamentals of analytical chemistry. 8th ed. Belmont,CA: Brooks/Cole.

Solasi, R., Zou, Y., Huang, X., Reifsnider, K. & Condit, D. 2007. On mechanical behaviour and in-plane modeling of constrained PEM fuel cell membranes subjected to hydration and temperature cycles. *Journal of Power Sources,* 167:366-377.

Solasi, R., Huang, X. & Reifsnider, K. 2010. Creep and stress-rupture of Nafion® membrane under controlled environment. *Mechanics of Materials,* 42:678-685.

Sun, J., Lian, Y., Li, Y., He, X. & Zheng,Z. 2014. Closed-form solution of elastic circular membranes with initial stress under uniformly-distributed loads: Extended Hencky solution. *Wiley Online Library.*

Tang, H., Peikan, S., Jiang, S.P., Wang, F. & Pan, M. 2007. A degradation study of Nafion® proton exchange membrane of PEM fuel cells. *Journal of Power Sources,* 170:85-92.

Tang, Y.L., Karlsson, A.M., Santare, M.H., Gilbert, M., Cleghorn, S. & Johnson, W.B. 2006. An experimental investigation of humidity and temperature effects on the mechanical properties of perfluorosulfonic acid membrane. *Materials Science and Engineering a-Structural Materials Properties Microstructure and Processing*, 425:297-304.

Thomassem, M., Sheridan, E. & Kvello, J. 2010. Electrochemical hydrogen separation and compression using polybenzimidazole (PBI) fuel cell technology. *Journal of Natural Gas Science and Engineering,* 2:229-234.

Vengatesan, S., Fowler, M.W., Yuan, X. & Wang, H. 2011. Diagnosis of MEA degradation under accelerated relative humidity cycling. *Journal of Power Sources,* 196:5045-5052.

Wan, K., Guo, S. 7 Dillard, D.A. 2003. A theoretical and numerical study of a thin clamped circular film under an external load in the presence of a tensile residual stress. *Thin Solid Films,* 425:150-162.

Werner, S., Jorissen, L. & Heider, U. 1996. Conductivity and mechanical properties of recast Nafion® films. *Ionics,* 2(1):19-23.

Wu, C.L., Fang, W. And Yip, M. 2000. Measurement of mechanical properties of thin films using bulge test. *Department of Power Mechanical Engineering National Tsing Hua University.*

Wu, J., Yuan, X.Z., Martin, J.J., Wang, H., Zhang, J., Shen, J., Wu, S. & Merida, W. 2008. A review of PEM fuel cell durability: Degradation mechanisms and mitigation strategies. *Journal of Power Sources,* 184:104-119.

Yang, J., Sudik, A., Wolverton, C. & Siegel, D.J. 2010. High capacity hydrogen storage materials: Attributes for automotive applications and techniques for material discovery. *Chemical Society Reviews,* 39:656-675.

Zhang, J., Tang, Y., Song, C., Cheng, X. & Wang,H. 2007. PEM fuel cells operated at 0% relative humidity in the temperature range of 23-120℃. *Electrochemical Acta,* 52:5095-5101.

Zhang, H. & Shen, P.K. 2012. A brief consideration about the structural evolution of perfluorosulfonic-acid ionomer membranes. *International Journal of Hydrogen Energy,* 37:4657-4664.

List of Appendices

Appendix A. Mathematical method

Membranes are essentially categorised as thin or thick according to their thickness with the thickness typically ranging between 0.5 - 500 μm. The lower limit for membrane thickness is defined by the possibilities of fabrication. Membranes with a thickness of 0.5 μm are extremely hard to manufacture without holes and generally cannot withstand usual loads. Therefore, the lower limit for membrane thickness is regarded as 0.5 μm. The upper limit is given by fact that thicker membranes are no longer a microscopic element and is regarded as 500 μm as a result. A membrane is classified as thick when its maximum deflection, w_0, is much smaller than its thickness, R_M, and as thin when the deflection is larger than the thickness.

The methodology of the behaviour and property determination of thin Nafion® membranes are based on Figure 2.2.

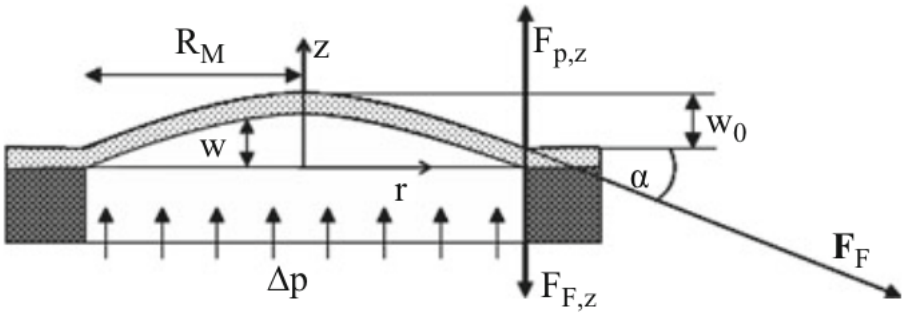

Figure 2.2 - Cross section of a pressure loaded circular thin membrane (Taken from Schomburg(2011)).

During pressurised blister testing/bulge testing the membrane loaded in high pressure cell is subjected to a pressure change, resulting in a deflection of the membrane across the exposed area. According to Hooke's law, as the membrane is deflected, its neutral finer needs to become longer, resulting in strain across the matrix that generates stress. The deflection curve of a thin circular membrane can therefore be describe by the following equation:

$$w(r) = w_0\left(1 - \frac{r^2}{R^2}\right) \qquad \text{(Eq.A.1)}$$

In the case where a circular membrane is clamped to prevent lateral movement when a constant pressure increase, ΔP, is applied, the deflection can be calculated from the equilibrium forces at the rim. The total force, F_p, acting on the membrane is equal to the product of the pressure difference and the exposed membrane area. This force is balanced by the force of the frame fixing the membrane to the circumference, F_F. Because the membrane is fixed in a frame, there is no lateral movement during pressurisation, therefore the lateral components of this cancel out when summed across the entire rim. The vertical components, $F_{p,z}$ and $F_{F,z,}$ of the applied pressure and the force of the frame respectively, are in equilibrium.

$$F_{P,z} = \Delta P \pi R_M^2 = -F_{F,z} = -\sigma_M d_M 2\pi R_M \sin(\alpha) \quad \text{(Eq.A.2)}$$

The product of the stress in the membrane during pressurisation, σ_M, and the cross-sectional area around the circumference, which is a product of the membrane thickness and the length circumference, $2\pi R_m$, gives the force of the frame. The vertical component can therefore be obtained by multiplying the force of the frame with the sine of the angle at which the membrane touches the frame. When the angle, α, is small, the sine is approximately the same as the slope of the membrane at the rim, which is equal to the tangent of α, and can be calculated as the derivative of the deflection curve w(r) at the rim. Therefore, Equation A.2 becomes:

$$\Delta P \pi R_M^2 = -\sigma_M d_M 2\pi R_M \tan(\alpha) = -\sigma_M d_M 2\pi R_M \left.\frac{\partial w}{\partial r}\right|_{r=R_M} \quad \text{(Eq.A.3)}$$

The curvature described by Equation A.1 is the deflection curve of the membrane. Thus, by calculating the derivative of this, substituting into Equation A.3 and solving for the pressure drop results in:

$$\Delta P \pi R_M^2 = -\sigma_M d_M 2\pi R_M w_0 \frac{2}{R_M} = 4\pi w_0 d_M \sigma_M \quad \text{(Eq.A.4)}$$

And therefore:

$$\Delta P = \frac{4 w_0 d_M}{R_M^2} \sigma_M \quad \text{(Eq.A.5)}$$

The stress, σ_M, of the membrane due to the applied pressure consists of three parts i.e. the residual stress, σ_0, which is present prior to any deflection of the membrane, the stress due to bending moments and the stress generated due to the stretching of the neutral fibre. The stress due to deflection can be calculated from the strains in the radial and tangential directions, ε_R and ε_T respectively. The radial strain, according to Hooke's law, can be calculated as:

$$\varepsilon_R = \frac{\sigma_R}{\mathrm{E}_M} + v_M \frac{\sigma_T}{\mathrm{E}_M} = \frac{1}{\mathrm{E}_M}\left(\sigma_R + v_M \sigma_T\right) \quad \text{(Eq.A.6)}$$

The strain generated by the radial stress is shown by the first term of Equation A.6 and the second term shows the transverse strain due to tangential stress of the membrane. The Young's modulus and Poisson's ratio is denoted by E_M and v_M respectively. Additionally, in accordance with Equation A.6 the tangential strain can be calculated as:

$$\varepsilon_T = \frac{\sigma_T}{\mathrm{E}_M} + v_M \frac{\sigma_R}{\mathrm{E}_M} = \frac{1}{\mathrm{E}_M}\left(\sigma_T + v_M \sigma_R\right) \quad \text{(Eq.A.7)}$$

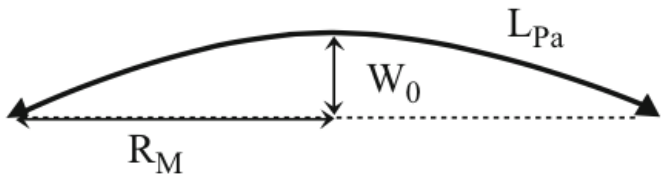

Figure 2.3 - Length of a parabola as a result of deflection.

The radial strain is estimated by the extension of the membrane across its neutral fibre, which is necessary for deflection to occur. For thin membranes it can be assumed that the radial strain is constant over the entire membrane as bending moments do not occur. The length of the curvature during deflection can be calculated as:

$$L_{Pa} \approx 2R_M \left(1 + \frac{2}{3}\frac{w_0^2}{R_M^2} - \frac{2}{5}\frac{w_0^4}{R_M^4} \right) \qquad \text{(Eq.A.8)}$$

Therefore, the strain required to cause a deflection of which the base length is extended to the length of the parabola is:

$$\varepsilon_R \approx \frac{2}{3}\frac{w_0^2}{R_M^2} \qquad \text{(Eq.A.9)}$$

With the radial strain known, two boundary conditions are established:

1. The radial and tangential strains are equal, in the centre of the membrane, due to the fact that the strain is not a function of direction at this position because of symmetry.
2. The tangential strain is zero at the circumference, because the membrane is clamped in a fixed position preventing any movement.

If the tangential and radial strains are assumed to be constant over the entire membrane, Equation A.6 can be transformed to give:

$$\sigma_R = \varepsilon_R \frac{\mathrm{E}}{1 - v_M} \qquad \text{(Eq.A.10)}$$

However, if the tangential strain is assumed to be zero over the entire membrane, it is found that:

$$\sigma_R = \varepsilon_R \frac{\mathrm{E}}{1 - v_M^2} \qquad \text{(Eq.A.11)}$$

For most materials, the Poisson's ration is a constant value of ±0.3 (Li *et al.,* 2009). However, due to the fact that polymer membranes adsorbs/desorbs water the value of Poisson's ration can vary from 0.3 when the membrane is in a glassy (dry) state, to 0.5 when the membrane is in a rubbery

(wet) state. Because, the membranes are not subjected to contact with liquid water, and therefore not reaching a rubbery state, it can be assumed that Poisson's ration is constantly 0.4 during the experimental procedures (Li *et al.,* 2009 and Schomburg, 2011).

The potential energy of a membrane with thickness d_M, radius R_M, Young's modulus E_M, Poisson's ratio v_M and deflection can be calculated from a differential equation with the following form if the bending moments of the membrane, residual stress, the stress due to straining and pressure drop are all taken into account.

$$V_P = \int\int dxdy \left[\frac{\mathrm{E}_M d_M^3}{24\left(1-v_M^2\right)} \left(\frac{\partial^2 w}{\partial x^2} + \frac{\partial^2 w}{\partial y^2} \right)^2 + \frac{d_M}{2} \left(\sigma_{x0} \left\{ \frac{\partial w}{\partial x} \right\}^2 + \sigma_{y0} \left\{ \frac{\partial w}{\partial y} \right\}^2 \right) \right.$$

$$\left. + \frac{d_M}{8} \frac{\mathrm{E}_M}{1-v_M^2} \left(\left\{ \frac{\partial w}{\partial x} \right\}^4 + \left\{ \frac{\partial w}{\partial y} \right\}^4 \right) - w\Delta P \right] \qquad \text{(Eq.A.12)}$$

The first term in the brackets of the equation above corresponds to the effect of the bending moments, the second to the residual membrane stress in the radial and tangential directions, respectively, and third to the contribution of the stress due to the straining of the neutral fibre and the final term to the energy generated by moving the membrane at the pressure difference.

In principle, the deflection curve w(r) of the membrane would need to be found which yields the minimum potential energy. Instead, Schomburg (2011) used an ansatz chosen such that it describes the expected deflection cure as good as possible, rather than an unknown deflection curve. For a circular membrane with radius, R_M, and centre deflection, w_0, an ansatz with a fourth-order polynomial with the free parameters w_0, a_0, a_1, a_2, a_3 and a_4 is made:

$$w(r) = w_0 \left(a_0 + a_1 \frac{r}{R_M} + a_2 \frac{r^2}{R_M^2} + a_3 \frac{r^3}{R_M^3} + a_4 \frac{r^4}{R_M^4} \right) \qquad \text{(Eq.A.13)}$$

Some free parameters can be derived from boundary conditions: The slope of the membrane at its centre needs to be zero, i.e. the derivative of w(r) at r = 0 needs to be zero; therefore $a_1 = 0$. Also, the deflection at the centre of the membrane is defined to be w_0, resulting in $a_0 = 0$. Lastly, the deflection at the rim and the slope of the membrane at the rim are necessarily zero. By using these parameters, the following equations can be created:

$$a_2 = a_4 - 3 \text{ and } a_3 = 2 - 2a_4 \qquad \text{(Eq.A.14)}$$

As a consequence, w_0 and a_4 are the only free parameters remaining, as a_2 and a_3 are dependent on a_4, and Equation 13 becomes:

$$w(r) = w_0\left(1+\left[a_4-3\right]\frac{r^2}{R_M^2}+\left[2-2a_4\right]\frac{r^3}{R_M^3}+a_4\frac{r^4}{R_M^4}\right) \qquad \text{(Eq.A.15)}$$

where w_0 is the deflection at the centre of the membrane and a_4 is a measure of the deflection shape of the membrane. The case when $a_4 = 1$ corresponds to a circular, thick membrane. The figure shown below shows the deflection curve as a function of a4. A thin membrane would correspond to the parabola as shown on the figure. Obviously, an ansatz cannot model a parabola, because the slope is not zero at the rim. However, it can be used to make a very accurate approximation. Equation A.15 is now differentiated and the results inserted into Equation A.12. The integral can then be calculated because the resulting function is an polynomial equation.

$$V_P = \left[\frac{\mathrm{E}_M d_M^3}{24\left(1-v_M^2\right)}\frac{w_0^3}{R_M^2}\left(9+\frac{6}{5}a_4+\frac{7}{15}a_4^2\right)+\frac{d_M}{2}\sigma_{r0}w_0^2\left(\frac{3}{5}+\frac{2}{35}a_4+\frac{1}{105}a_4^2\right)\right.$$
$$+\frac{\mathrm{E}_M d_M}{24\left(1-v_M^2\right)}\frac{w_0^4}{R_M^2}\left(\frac{9}{70}+\frac{6}{385}a_4+\frac{3}{385}a_4^2+\frac{2}{5{,}005}a_4^3+\frac{1}{30{,}030}a_4^4\right)$$
$$\left.-\Delta P w_0 R_M^2\left(\frac{3}{20}+\frac{1}{60}a_4\right)\right] \qquad \text{(Eq.A.16)}$$

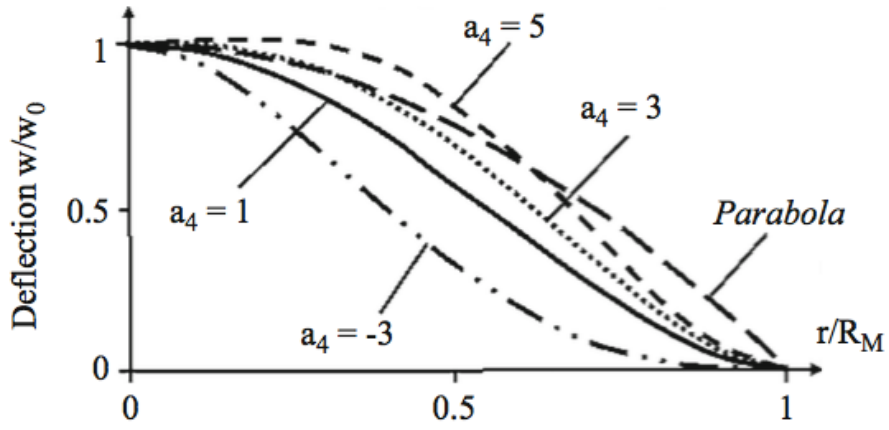

Figure 2.6 - Deflection curve of a circular membrane calculated with (20) as a function of a_4.

The potential energy of the membrane is described as a function of the free parameters w_0 and a_4 in the equation above. The minimum potential energy is found by calculating the the zero of the

derivative with respect to the corresponding parameter, *e.g*. the following system of two equations needs to be solved for w_0 and a_4:

$$0 = \frac{\partial V_P}{\partial a_4} = 2\pi\left[\frac{\mathrm{E}_M d_M^3}{24\left(1-v_M^2\right)} \frac{w_0}{R_M^2}\left(9 + \frac{6}{5}a_4 + \frac{7}{15}a_4^2 \right) + \frac{d_M}{2}\sigma_{r0} w_0 \right.$$
$$\cdot\left(\frac{3}{5} + \frac{2}{35}a_4 + \frac{1}{105}a_4^2 \right) + \frac{\mathrm{E}_M d_M}{\left(1-v_M^2\right)} \frac{4w_0^3}{R_M^2} \cdot \left(\frac{9}{70} + \frac{6}{385}a_4 + \frac{3}{385}a_4^2 \right.$$
$$\left. \left. + \frac{2}{5{,}005}a_4^3 + \frac{1}{30{,}030}a_4^4 \right) - \Delta P R_M^2 \left(\frac{3}{20} + \frac{1}{60}a_4 \right) \right] \qquad \text{(Eq.A.17)}$$

$$0 = \frac{\partial V_P}{\partial a_4} = 2\pi\left[\frac{\mathrm{E}_M d_M^3}{24\left(1-v_M^2\right)} \frac{w_0^2}{R_M^2}\left(\frac{6}{5} + \frac{7}{15}a_4 \right) + d_M \sigma_{r0} w_0^2 \cdot \left(\frac{1}{35}a_4 + \frac{1}{105}a_4 \right) \right.$$
$$\left. + \frac{\mathrm{E}_M d_M}{1-v_M^2} \frac{w_0^4}{R_M^2} \cdot \left(\frac{6}{385} + \frac{6}{385}a_4 + \frac{6}{5{,}005}a_4^2 + \frac{2}{15{,}015}a_4^3 \right) - \frac{\Delta P w_0 R_M^2}{60} \right]$$

(Eq.A.18)

There is a non-linear term due to the straining of the neutral fibre. If it is assumed that the parameter a_4 is always equal to one the only free parameter remaining is w_0 of the membrane. At the extremes of the potential energy, the derivative of the potential energy with respect to the deflection is zero:

$$0 = \frac{\partial V_p}{\partial w_0} = 2\pi\left(\frac{8}{3}\frac{\mathrm{E}_M d_M^3}{1-v_M^2}\frac{w_0}{R_M^2} + 2 d_M \sigma_0 w_0 + \frac{128}{105}\frac{\mathrm{E}_M d_M}{1-v_M^2}\frac{w_0^3}{R_M^2} - \frac{1}{2}\Delta P R_M^2 \right) = F_M \qquad \text{(Eq.A.19)}$$

The derivative of the potential energy with respect to the movement is the force, in general. Therefore, Equation A.18 is a description of the force F_M acting on the membrane, and the deflection where the force becomes zero corresponds to the equilibrium of forces. Solving Equation A.19 for the pressure drop over the membrane yields an equation which describes the correlation between the pressure drop and the deflection of the membrane:

$$\Delta P = \frac{4 d_M w_0}{R_M^2}\left(\frac{4}{3}\frac{d_M^2}{R_M^2}\frac{\mathrm{E}_M}{1-v_M^2} + \sigma_0 + \frac{64}{105}\frac{w_0^2}{R_M^2}\frac{\mathrm{E}_M}{1-v_M^2} \right) \qquad \text{(Eq.A.20)}$$

The three terms in the brackets of Equation A.19 corresponds to the contributions of bending moments, residual stress and stress due to straining of the neutral fibre respectively. The contributions of the bending moment and residual stress, respectively, can be considered to be

zero. This is a valid assumption as bending moments has little to no effect with the use of thin membranes, and as the membrane is clamped in a fixed position there is no initial residual stress (Schomburg, 2011, Li *et al.,* 2009 and Merle, 2013.). With regards to the above mentioned and Equation A.5, Equation A.20 can be rewritten as:

$$\Delta P = \frac{4 d_M w_0}{R_M^2}\left(\frac{64}{105}\frac{w_0^2}{R_M^2}\frac{\mathrm{E}_M}{1-v_M^2}\right) = \frac{4 d_M w_0}{R_M^2}\sigma_R \qquad \text{(Eq.A.21)}$$

The rupture pressure of a membrane calculated by calculating the maximum pressure drop. Therefore, it is required to determine the maximum radial stress the membrane can endure prior to rupture. The rupture pressure can thus be calculated as:

Appendix B. High-Pressure Cell Design

*Units presented in millimetres

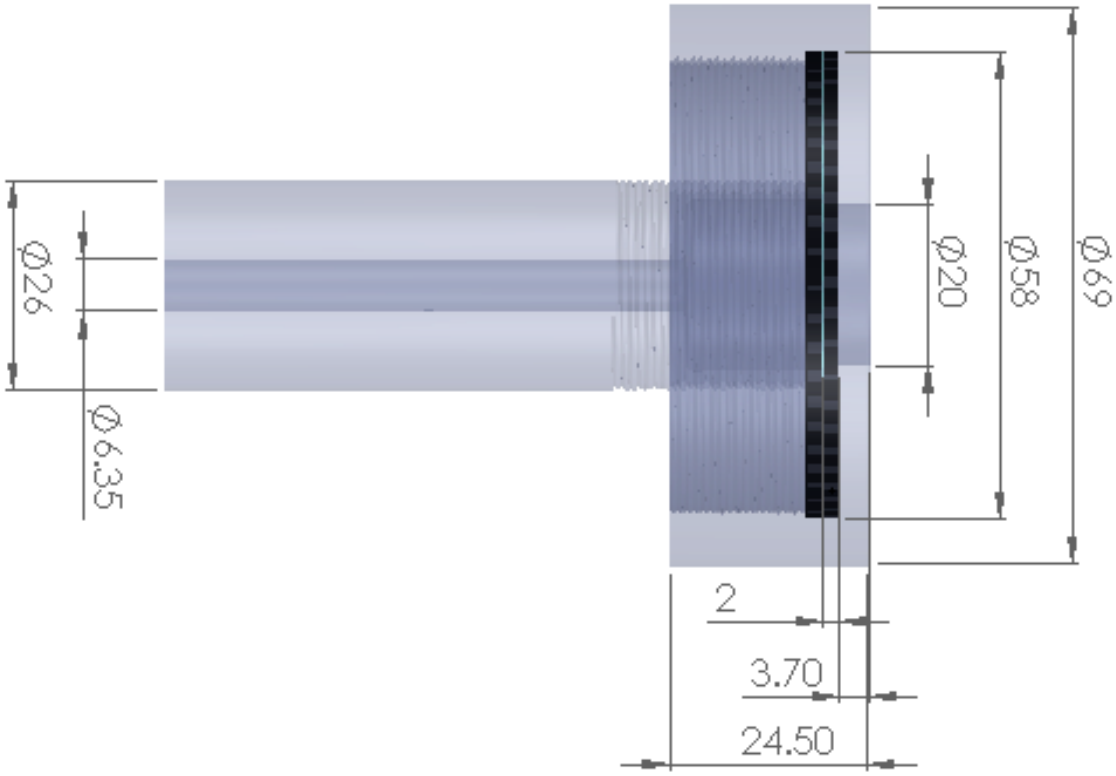

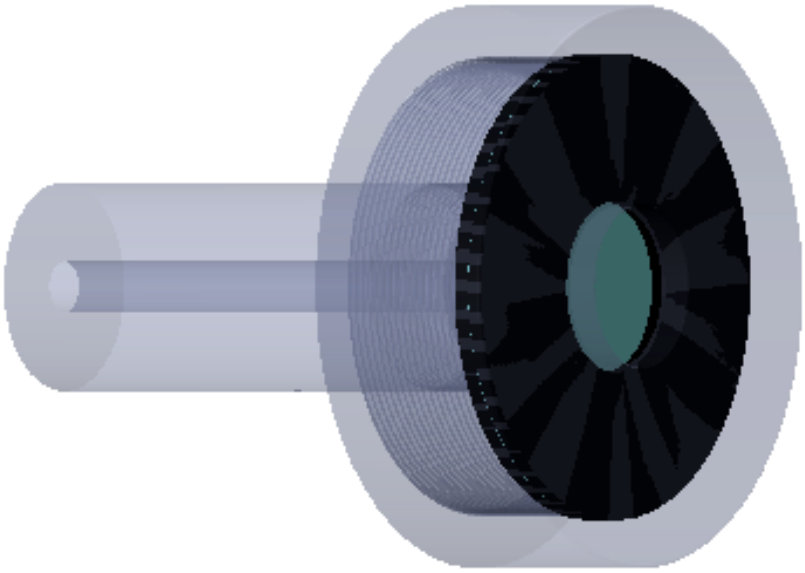

Appendix C. Equipment Schedule

Baseline Nitrogen gas: Nitrogen gas cylinders, supplied by Afrox, is used as baseline gas.

Environmental chamber: ESPEC SH-221, used to control the relative humidity and temperature that the membrane is exposed to. The chamber is capable of reaching temperatures and relative humidity level of -30℃ to 160℃ and 0% to 100% respectively. The chamber can be operated under constant operation or as a programmed operation.

High-pressure cell: Designed by the author of the thesis. Detailed schematic drawings are presented in Appendix C.

Needle valves: SWAGELOK, the first valve serves to control the gas flow rate or rate of pressurisation within the high-pressure cell, whilst the second serves as a purge valve ensuring the flow specifications of the thermal mass flow meter is not exceeded.

Pressure relief valves: Included as a safety precaution, insuring that overpressure is not possible during operation. Set to open at pressures exceeding 206 barg.

Pressure transducer: BD-SENSORS DMP-331. The pressure transducers are placed at different sections of the experimental setup, to ensure accurate readings of the pressure within the high-pressure cell. Two of the transducers are specified for pressures of 0 - 200 barg whilst the third is specified for 0 - 34 barg. The latter was included, as it provides a more stable signal at low pressures.

Solenoid valves: BÜRKERT Type-2400, used to control gas flow to the system. During the pressure cycling procedure, one solenoid valve is used to control gas flow to the system whilst the other is used to purge high-pressure gas.

Thermal mass flow meter: AALBORG GFM-17, used to measure the gas flow to determine the rate of pressurisation within the high-pressure cell.

Appendix D: Hazard and safety analysis

Introduction

Laboratory safety is of the utmost importance when experimental procedures are performed by individuals in the laboratory. Therefore, it is imperative that the individuals involved are aware of the hazards within the laboratory. The following laboratory rules and safety equipment were used.

Laboratory rules and safety equipment

General Rules

The following rules apply to all individuals entering the laboratory environment:

- No practical jokes or horse play allowed.
- All participants must behave in a responsible manner.
- Do not work with equipment that is beyond the scope of your project.
- No food and beverages allowed in the laboratory.
- Always exhibit good housekeeping practices.
- Participants must familiarise themselves with the environment and be acquainted with the location of safety equipment.

Safety equipment

The following safety equipment is provided to individuals working in the laboratory should be aware of its location at all times whilst applying general laboratory rules:

- Fire extinguishers.
- Emergency kit (small general injuries).
- Eye wash station.
- Safety shower.

Emergency contacts

The following numbers should be present in the laboratory at all times:

- (018) 299 211 – PUK department of protection services.
- (018) 293 1111 – Fire Brigade.
- 084 4124 – ER24.
- 0825 911 – NETCARE.

PPE

PPE that must be worn in the laboratory at all times include:

- Lab coats
- Safety goggles
- Long trousers
- Closed shoes

Appendix E. Calculation Examples

Calculation Of Young's modulus :

NR115 at 20℃ and 35% RH with the utilisation of a webcam.

Constants:

$d_M = 0.13$ mm

$R_M = 10$ mm

$v_M = 0.4$

Measured variables:

P = 0.519 MPa

$w_0 = 4.35$ mm

Calculate E_M

$$P = \frac{4 d_M w_0}{R_M^2}\left(\frac{4}{3}\frac{d_M^2}{R_M^2}\frac{E_M}{1-v_M^2} + \sigma_0 + \frac{64}{105}\frac{w_0^2}{R_M^2}\frac{E_M}{1-v_M^2}\right)$$

$$0.519 = \frac{(4)(0.13)(4.35)}{(10^2)}\left(\left(\frac{4}{3}\right)\left(\frac{0.13^2}{10^2}\right)\left(\frac{E_M}{1-0.4^2}\right) + 0 + \left(\frac{64}{105}\right)\left(\frac{4.35^2}{10^2}\right)\left(\frac{E_M}{1-0.4^2}\right)\right)$$

Solving for E_M :

$E_M = 196$ MPa

Constants:

$d_M = 0.13$ mm

$R_M = 10$ mm

$\nu_M = 0.4$

$\mathrm{E}_M = 196$ MPa

Measured variables:

$L_{Pa} = 22.2$ mm

Calculate w_0 & P

$$L_{Pa} = 2R_M\left(1+\frac{2}{3}\frac{w_0^2}{R_M^2}-\frac{2}{5}\frac{w_0^4}{R_M^4}\right)$$

$$22.2 = (2)(10)\left(1+\left(\frac{2}{3}\right)\left(\frac{w_0^2}{10^2}\right)-\left(\frac{2}{5}\right)\left(\frac{w_0^4}{10^4}\right)\right)$$

Solving for w_0:

$w_0 = 4.31$ mm

$$P = \frac{4d_M w_0}{R_M^2}\left(\frac{4}{3}\frac{d_M^2}{R_M^2}\frac{\mathrm{E}_M}{1-\nu_M^2}+\sigma_0+\frac{64}{105}\frac{w_0^2}{R_M^2}\frac{\mathrm{E}_M}{1-\nu_M^2}\right)$$

$$P = \frac{(4)(0.13)(4.31)}{(10^2)}\left(\left(\frac{4}{3}\right)\left(\frac{0.13^2}{10^2}\right)\left(\frac{196}{1-0.4^2}\right)+0+\left(\frac{64}{105}\right)\left(\frac{4.31^2}{10^2}\right)\left(\frac{196}{1-0.4^2}\right)\right)$$

Solving for P :

$P = 0.506$ MPa

Comparison of deflection measuring methods:

From the measurement of the curvature of NR115 at 20℃ and 35% RH, it is possible to calculate the deflection and from there the rupture pressure or Young's modulus if so desired. The calculations are displayed below with comparison between the curvature measurement and the visual webcam method presented in Table E1.

A slight difference in the values of the rupture pressures are observed for the two methods. Method 1, the use of the webcam, is considered to be the more accurate of the two methods, as all values are determined with visual aid. Method two, the measurement of the curvature length, is a slightly more theoretical method, but can be considered as a valid method for the determination of the membrane deflection as the calculated values fall within the experimental error range of 6%.

The use of a webcam was implemented in this study, as it ensured a grater degree of control over calculations and also eliminates the possibility of wasting valuable membrane samples.

Table E1 - Comparison of methods used to determine membrane deflection during experimental operation.

	Webcam	**String**
L_{Pa} (mm)	n.a.	22.2
w_0 (mm)	4.35	4.31
P (kPa)	519	506

Appendix F Repeatability and statistical analysis

F1. Repeatability

The repeatability of the system and experimental method was validated by performing ten rupture tests on Nafion® 115 membrane samples at 50℃ and a relative humidity level of 10%. As the entire system is automated, the possibility of human error is minimised, allowing for accurate, repeatable measurements. The results of the repeatability validation are presented in Figure F1 below.

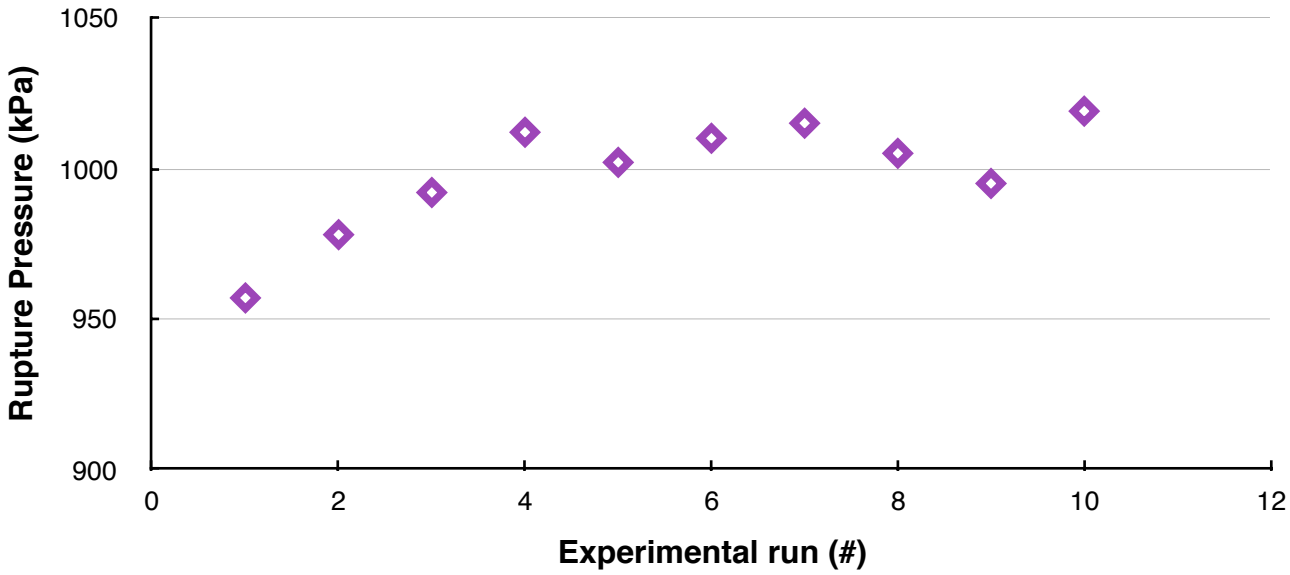

Figure F1. - Repeatability of system through rupture tests on Nafion® 115 at 50℃ and 10% RH.

A statistical regression analysis was performed in Microsoft Excel using the data as shown in Figure F1 to determine the experimental percentage error over the entire data series within a 95% confidence level. The results of the statistical regression analysis are provided in Appendix F2. The experimental error percentage was calculated as 6%. .

F2. Regression Analysis

SUMMARY OUTPUT

Regression Statistics	
Multiple R	0.187
R Square	0.035
Adjusted R Square	-0.085
Standard Error	**6%**
Observations	10.000

ANOVA

	df	*SS*	*MS*	*F*	*Significance F*
Regression	1	0.01150	0.01150	0.29144	0.60400
Residual	8	0.31566	0.03946		
Total	9	0.32716			

	Coefficients	*Standard Error*	*t Stat*	*P-value*	*Lower 95%*	*Upper 95%*	*Lower 95.0%*	*Upper 95.0%*
Intercept	9.989	**6%**	159.016	0	9.844	10.133	9.844	10.133
X Variable 1	0	0	65535		0	0	0	0